Differential requirements of androgen receptor in luminal progenitors during prostate regeneration and tumor initiation

Chee Wai Chua[1,4], Nusrat J. Epsi[2], Eva Y. Leung[1], Shouhong Xuan[1], Ming Lei[1], Bo I. Li[1], Sarah K. Bergren[1], Hanina Hibshoosh[3], Antonina Mitrofanova[2], and Michael M. Shen[1]*

[1]Departments of Medicine, Genetics & Development, Urology, and Systems Biology, Herbert Irving Comprehensive Cancer Center, Columbia University Medical Center, New York, NY 10032

[2]Department of Health Informatics, Rutgers School of Health Professions, Rutgers Biomedical and Health Sciences, Rutgers, The State University of New Jersey, Newark, NJ 07103

[3]Department of Pathology and Cell Biology, Herbert Irving Comprehensive Cancer Center, Columbia University Medical Center, New York, NY 10032

[4]Present address: [1]State Key Laboratory of Oncogenes and Related Genes, Renji-Med X Clinical Stem Cell Research Center, Ren Ji Hospital, School of Medicine, Shanghai Jiao Tong University, Shanghai, 200240, China; and [2]Department of Urology, Ren Ji Hospital, School of Medicine, Shanghai Jiao Tong University,

*Author for correspondence at:

Phone: (212) 851-4723; fax: (212) 851-4572; e-mail: mshen@columbia.edu

Abstract

Master regulatory genes of tissue specification play key roles in stem/progenitor cells and are often important in cancer. In the prostate, androgen receptor (AR) is a master regulator essential for development and tumorigenesis, but its specific functions in prostate stem/progenitor cells have not been elucidated. We have investigated AR function in CARNs (CAstration-Resistant Nkx3.1-expressing cells), a luminal stem/progenitor that functions in prostate regeneration. Using genetically-engineered mouse models and novel prostate epithelial cell lines, we find that progenitor properties of CARNs are largely unaffected by AR deletion, apart from decreased proliferation *in vivo*. Furthermore, AR loss suppresses tumor formation after deletion of the *Pten* tumor suppressor in CARNs; however, combined *Pten* deletion and activation of oncogenic *Kras* results in AR-negative tumors with focal neuroendocrine differentiation. Our findings show that AR modulates specific progenitor properties of CARNs, including their ability to serve as a cell of origin for prostate cancer.

Introduction

Elucidating the cell type(s) of origin of cancer and the molecular drivers of tumor initiation is of fundamental importance in understanding the basis of distinct tumor subtypes as well as differences in treatment response and patient outcomes (Blanpain, 2013; Rycaj and Tang, 2015; Shibata and Shen, 2013; Visvader, 2011). Furthermore, since cancer often originates from stem cells and/or lineage-restricted progenitor cells, the identification of stem/progenitor cells is of considerable significance. In the case of the prostate, however, both the specific identity of stem/progenitor cells as well as cell types of origin for cancer have remained unclear (Lee and Shen, 2015; Wang and Shen, 2011; Xin, 2013).

In the normal prostate epithelium, there are three primary cell types, corresponding to secretory luminal cells, an underlying layer of basal cells, and rare neuroendocrine cells (Shen and Abate-Shen, 2010; Toivanen and Shen, 2017). Lineage-tracing studies have shown that both luminal and basal cells are mostly lineage-restricted (unipotent) in the normal adult mouse prostate as well as during androgen-mediated prostate regeneration (Choi et al., 2012; Liu et al., 2011; Lu et al., 2013; Wang et al., 2013). In addition, cells within the basal compartment possess stem/progenitor properties in a range of *ex vivo* assays as well as during inflammation and wound repair (Goldstein et al., 2008; Hofner et al., 2015; Kwon et al., 2014; Lawson et al., 2007; Toivanen et al., 2016; Wang et al., 2013). However, recent studies have shown that luminal cells can also display stem/progenitor properties in specific *in vivo* and *ex vivo* contexts (Chua et al., 2014; Karthaus et al., 2014; Kwon et al., 2016; Wang et al., 2009). Furthermore, there is now considerable evidence supporting a luminal origin for prostate cancer, both in mouse models (Wang et al., 2009; Wang et al., 2014) as well as in human tissues (Gurel et al., 2008; Meeker et al., 2002).

Androgen receptor (AR) plays a central role in many aspects of normal prostate development as well as prostate cancer progression (Cunha et al., 2004; Toivanen and Shen, 2017; Watson et al., 2015). In the prostate epithelium of adult hormonally-intact mice, AR is

primarily expressed by luminal cells, but is also found in a subset of basal cells (Lee et al., 2012; Mirosevich et al., 1999; Xie et al., 2017). Several studies have shown that conditional deletion of AR in the adult prostate epithelium results in a short-term increase in proliferation of luminal cells (Wu et al., 2007; Xie et al., 2017; Zhang et al., 2016a), indicating a role for AR in normal prostate homeostasis. Importantly, AR can act as a master regulator of prostate epithelial specification in a fibroblast reprogramming assay (Talos et al., 2017).

In the context of prostate cancer, tumor recurrence after androgen-deprivation therapy is due to the emergence of castration-resistant prostate cancer (CRPC), which is associated with increased AR activity that can be targeted by second-generation anti-androgen therapies (Watson et al., 2015). However, treatment failure following such anti-androgen therapies is frequently associated with the appearance of AR-negative tumor cells, which are typically associated with highly aggressive lethal disease (Beltran et al., 2014; Vlachostergios et al., 2017; Watson et al., 2015). In some cases, this AR-negative CRPC contain large regions displaying a neuroendocrine phenotype (CRPC-NE) (Beltran et al., 2016; Beltran et al., 2014; Ku et al., 2017; Mu et al., 2017; Zou et al., 2017).

Previous work from our laboratory has identified CARNs as a luminal stem/progenitor cell within the androgen-deprived normal mouse prostate epithelium that is also a cell of origin for prostate cancer (Wang et al., 2009). Following androgen administration to induce prostate regeneration, CARNs can generate both luminal and basal progeny *in vivo,* as well as in renal grafting and organoid assays (Chua et al., 2014; Wang et al., 2009). Although CARNs express AR (Wang et al., 2009), it has been unclear whether AR is required for any or all of the progenitor properties of CARNs, and whether the intrinsic castration-resistance of untransformed CARNs might resemble the castration-resistance of tumor cells in CRPC. Below, we show that the progenitor properties of CARNs are largely unaffected by loss of AR, whereas their ability to serve as cells of origin for prostate cancer are altered by AR deletion in a context-dependent manner. Notably, cell lines derived from AR-deleted CARNs have molecular profiles that

resemble those for CRPC, and AR-deleted CARNs can serve as a cell of origin for focal neuroendocrine differentiation in a novel mouse model of AR-negative prostate cancer.

Results

To investigate whether the stem/progenitor properties of CARNs are dependent upon AR function, we have used an inducible targeting approach in genetically-engineered mice. For this purpose, we used mice carrying a conditional allele of *Ar* (De Gendt et al., 2004) together with the inducible *Nkx3.1*^{CreERT2} driver (Wang et al., 2009) and the *R26R-YFP* reporter to visualize cells and their progeny in which Cre-mediated recombination has taken place (Srinivas et al., 2001); as *Ar* is an X-linked gene, deletion of a single allele in males is sufficient to confer a hemizygous null phenotype. Since CARNs are Nkx3.1-expressing cells found under androgen-deprived conditions, we castrated adult male mice carrying the Cre driver and reporter alleles, followed by tamoxifen induction to induce Cre-mediated activity specifically in CARNs (Figure 1A).

Using this strategy, we compared the properties of CARNs in *Nkx3.1*$^{CreERT2/+}$*; R26R-YFP/+* mice, which we denote as "control" mice, with those in *Nkx3.1*$^{CreERT2/+}$*;* *Ar*$^{flox/Y}$*; R26R-YFP/+* mice, which we denote as "AR-deleted" mice. We found that the percentage of lineage-marked YFP-positive cells, corresponding to CARNs, was not significantly different (p=0.51) between the control (0.36 ± 0.17%, n=5 mice) and AR-deleted mice (0.31 ± 0.06%, n=5 mice) (Figure 1B, C). Notably, we found that 87.1% of the YFP-positive cells in *Nkx3.1*$^{CreERT2/+}$*;* *Ar*$^{flox/Y}$*; R26R-YFP/+* mice (n=344/395 cells in 4 mice) were AR-negative, indicating that AR deletion occurred with high efficiency. Furthermore, these YFP-positive cells expressed the luminal markers cytokeratins 8 and 18 (CK8 and CK18), but not cytokeratin 5 (CK5) and p63, indicating that AR deletion does not alter the luminal phenotype of CARNs (Figure 1D). These findings indicate that AR deletion does not affect the frequency or luminal properties of CARNs.

To investigate the progenitor properties of AR-deleted CARNs, we examined their ability to generate progeny during androgen-mediated regeneration. We implanted subcutaneous mini-osmotic pumps containing testosterone into control *Nkx3.1*$^{CreERT2/+}$*; R26R-YFP/+* mice as well as *Nkx3.1*$^{CreERT2/+}$*;* *Ar*$^{flox/Y}$*; R26R-YFP/+* mice, followed by tissue harvest at 4, 7, 14, and 28 days

later; the final 28-day time point corresponds to a fully-regenerated prostate (Figure 2A). We found that the YFP-marked cells and cell clusters were similar in the control and AR-deleted prostates at 4 and 7 days after testosterone administration (Figure 2B, C). However, at 14 and 28 days, the control prostates contained many YFP-expressing cell clusters with more than 4 cells, whereas the prostates with AR-deleted CARNs mostly contained YFP-expressing single cells or doublets (Figure 2B, C).

To compare the proliferative ability of control and AR-deleted CARNs and their progeny, we pursued BrdU pulse-chase experiments during prostate regeneration. We performed castration and tamoxifen administration on control and AR-deleted mice, followed by androgen-mediated regeneration for 28 days, with administration of daily doses of BrdU either from days 1 through 4 of regeneration or from days 11 through 14 (Figure 3A, B). When BrdU was administered from days 1 through 4 of regeneration, we could readily detect $BrdU^+YFP^+$ cells in the control prostates (50.9 ± 11.8%, n=3 mice) as well as AR-deleted prostates (62.9 ± 14.9%, n=3 mice) (Figure 3C, E). In contrast, when BrdU was administered from days 11 through 14, we could only detect $BrdU^+YFP^+$ cells in the control prostates (11.1 ± 6.2%, n=3 mice), but not in the AR-deleted prostates (0%, n=3 mice) (Figure 3D, F). This difference suggests that AR-deleted CARNs and/or their progeny have a defect in proliferation during later stages of regeneration, consistent with the analysis of YFP^+ cluster size (Figure 2B).

Notably, although YFP-expressing basal cells could be readily identified in both control and AR-deleted prostates, there was an increase in the percentage of basal cells within the YFP^+ population in the AR-deleted mice (Figure 2D). This difference was evident using either the basal marker CK5 (2.1% $CK5^+AR^+YFP^+$ versus 19.2% $CK5^+AR^-YFP^+$) or p63 (3.5% $p63^+AR^+YFP^+$ versus 14.6% $p63^+AR^-YFP^+$) (Figure 2D). These findings indicate that AR-deleted CARNs favor generation of basal progeny, and/or that there is decreased proliferation or survival of luminal progeny during regeneration.

As a further test of the progenitor properties of AR-deleted CARNs, we examined their ability to generate prostate ducts in a tissue recombination/renal grafting assay. Previously, we had shown that single CARNs were capable of generating ducts in this assay (Wang et al., 2009). We isolated YFP-positive cells from control and AR-deleted mice that had undergone castration and tamoxifen induction, and recombined 10 YFP-positive cells together with 2.5 x 10^5 rat embryonic urogenital mesenchyme cells, followed by renal grafting (Figure 3G). We found that both control and AR-deleted CARNs could generate prostate ducts (Figure 3H), but that the AR-deleted CARNS were significantly less efficient (12.5% graft efficiency, n=16) compared to the control CARNs (p=0.003; 68.8% graft efficiency, n=16), consistent with a proliferation defect in the AR-deleted CARNs.

Based on these findings, we further investigated the properties of CARNs and AR-deleted CARNs by establishing adherent cell lines. Using a novel method based on conditions that we previously established for culture of prostate organoids (Chua et al., 2014), we successfully generated adherent cell lines from single YFP^+ cells isolated from castrated and tamoxifen-treated *Nkx3.1*$^{CreERT2/+}$*; Ar*$^{flox/Y}$*; R26R-YFP/+* mice. Genotyping of the resulting lines led to identification of *Ar*-positive (non-recombined allele) and *Ar*-negative (recombined allele) lines, which we term APCA and ADCA (Ar-Positive CArn-derived and Ar-Deleted CArn-derived) lines. These cell lines could be propagated as adherent cells in the presence of Matrigel and DHT. Under these conditions, we found that the APCA (n=2) and ADCA (n=2) lines were morphologically indistinguishable (Figure 4A). These cell lines were comprised of a mixture of cells expressing basal (CK5) or luminal (CK8) markers or both, as well as Foxa1, an epithelial marker that encodes a transcriptional partner of AR (Gao et al., 2003; He et al., 2010) (Figure 4A). Furthermore, both the APCA and ADCA lines showed robust proliferation at similar levels, as demonstrated by Ki67 immunostaining, CellTiter-Glo assays, and colony formation in the presence or absence of DHT (Figure 4A-C).

To determine the relative efficiency of forming APCA and ADCA lines from AR^+ and AR^- CARNs, respectively, we sorted 60 single YFP^+ cells from castrated and tamoxifen-treated *Nkx3.1*$^{CreERT2/+}$*; Ar*$^{flox/Y}$*; R26R-YFP/+* mice into individual wells of a 96-well plate. We found that 6 YFP^+ cells gave rise to adherent lines, with 4 of these corresponding to AR^+ lines that had failed to undergo Cre-mediated recombination of the conditional *Ar* allele, and 2 lines corresponding to AR^- lines. After correcting for the 87.1% efficiency of recombination of the AR-floxed allele *in vivo*, these data indicate that the relative plating efficiency for the AR^- CARNs compared to AR^+ CARNs is 7.4%, consistent with the decreased grafting efficiency of AR^- CARNs.

Notably, we were also able to use this methodology to establish 14 primary human prostate epithelial cell lines from benign prostatectomy specimens at high efficiency. Similar to the mouse APCA cell lines, these HPE (Human Prostate Epithelial) cell lines are propagated as adherent cells in the presence of Matrigel and DHT. All of these lines display similar marker phenotypes, expressing basal and luminal markers as well as AR and PSA, and are highly proliferative (Figure 4 – figure supplement 1).

To assess the ability of the APCA and ADCA cell lines to reconstitute prostate ducts, we performed tissue recombination assays by combining 1 x 10^5 cells with rat urogenital mesenchyme followed by renal grafting. We found that the APCA lines could generate prostate ducts (n=10 grafts with 2 lines; 100% efficiency), some with evidence of secretions, whereas the ADCA lines (n=6 grafts with 1 line; 67% efficiency) generated ducts that lacked prostate secretions (Figure 4D). Next, we tested the role of AR in this tissue reconstitution assay by treating the mice grafted with APCA cells (n=12 grafts with 2 lines) with tamoxifen at 7 weeks after grafting in order to induce *Ar* deletion. We found that tamoxifen treatment resulted in grafts containing prostate ducts composed of a mixture of AR-positive and negative cells, but with a decreased efficiency of graft formation relative to the same APCA lines in the absence of tamoxifen (42% versus 100% efficiency) (Figure 4D). Taken together, these results show that

AR deletion decreases the efficiency of prostate duct formation by CARN-derived cells, consistent with the results obtained using AR-deleted CARNs (Figure 3H). Notably, since ADCA cells do not display a growth disadvantage relative to APCA cells in culture, this difference in duct formation is likely to be due to a non-cell-autonomous effect mediated by the urogenital mesenchyme in grafts.

To examine the molecular basis for differences between the ADCA and APCA lines (n=2 lines each), we performed RNA-sequencing followed by bioinformatic analyses. Based on the RNA expression profiling data, we constructed a differential expression signature comparing ADCA cells to APCA cells. Using the resulting ADCA signature to examine pathway enrichment by Gene Set Enrichment Analysis (GSEA) (Subramanian et al., 2005), we found up-regulation of gene sets involved in DNA replication and repair pathways, as well as cell cycle and apoptosis (Figure 5A), suggesting that cellular proliferation and survival are affected by AR deletion. We also compared the ADCA signature with a signature defined between expression profiles of AR-null and AR-positive mouse prostate luminal cells (Xie et al., 2017), and found enrichment for up-regulated genes (Figure 5B). Next, we performed a cross-species comparison of the ADCA signature with a signature defined between profiles of human prostate luminal and basal epithelial cells (Zhang et al., 2016b), and found that there was no significant enrichment in either tail (Figure 5C), indicating that AR deletion does not drive APCA cells towards a specific lineage. Furthermore, we performed GSEA comparisons of the ADCA signature with several signatures obtained from analyses of human prostate cancer progression. In particular, we observed enrichment for up-regulated genes when compared to a signature of castration-resistant prostate cancer (CRPC) from Best and colleagues (Best et al., 2005), as well as to a signature of metastatic CRPC from Stanbrough and colleagues (Stanbrough et al., 2006) (Figure 5D, E). Moreover, we observed a strong enrichment when compared to a signature from Beltran and colleagues (Beltran et al., 2016) defined between CRPC with neuroendocrine differentiation (CRPC-NE) and non-neuroendocrine CRPC (Figure 5F), consistent with our observation of

pathway enrichment for gene sets corresponding to axon guidance and small-cell lung cancer (Figure 5A).

Finally, we tested the ability of AR-deleted CARNs to serve as a cell of origin for prostate cancer, based on the previous finding that prostate cancer can initiate from CARNs after specific deletion of *Pten* and androgen-mediated regeneration (Wang et al., 2009). We used *Nkx3.1*$^{CreERT2/+}$*; Pten*$^{flox/flox}$*; R26R-YFP/+* controls (which we term NP-CARN) and *Nkx3.1*$^{CreERT2/+}$*; Pten*$^{flox/flox}$*; Ar*$^{flox/Y}$*; R26R-YFP/+* mice (NPA-CARN) in an experimental paradigm involving castration, tamoxifen-treatment, and androgen-mediated regeneration for one month. We found that AR deletion resulted in a significant difference between the NP-CARN and NPA-CARN phenotypes, as the NP-CARN controls displayed high-grade prostatic intraepithelial neoplasia (PIN) whereas the NPA-CARN prostates showed a weak phenotype corresponding to diffuse hyperplasia with mild inflammation and increased apoptosis, (Figure 6A). The NPA-CARN prostates contained YFP-positive cells that also expressed phospho-Akt (pAkt), indicating successful deletion of *Pten*, but these cells were only found as solitary or as small clusters, unlike the large clusters of YFP^+pAkt^+ cells observed in the control NP prostates (Figure 6A). Furthermore, the NPA-CARN prostates displayed a decreased proliferative index relative to NP-CARN (2.7%, n=3 vs. 9.2%, n=3), as well as increased apoptosis (2.6%, n=3 vs. 0.7%, n=3) (Figure 6B). Taken together, findings indicate that AR is required for tumor initiation following *Pten* deletion in CARNs.

In contrast, AR deletion did not affect tumor initiation following combined deletion of *Pten* and activation of the oncogenic *Kras*^{G12D} allele. Using a similar protocol for castration, tamoxifen-treatment, and androgen-mediated regeneration, we compared the phenotypes of *Nkx3.1*$^{CreERT2/+}$*; Pten*$^{flox/flox}$*; Kras*$^{LSL\text{-}G12D/+}$*; R26R-YFP/+* controls (NPK-CARN) and *Nkx3.1*$^{CreERT2/+}$*; Pten*$^{flox/flox}$*; Kras*$^{LSL\text{-}G12D/+}$*; Ar*$^{flox/Y}$*; R26R-YFP/+* mice (NPKA-CARN). In both genotypes, deletion of *Pten* and activation of oncogenic *Kras* resulted in formation of tumors with large clusters of YFP^+ cells that express pAkt and Ras (Figure 6C). Furthermore, both NPK-

CARN and NPKA-CARN tumors displayed high proliferative indices (20%, n=3 vs. 19%, n=3) and low frequencies of apoptosis (0.9%, n=3 vs. 0.8%, n=3) (Figure 6D). Notably, we observed an important difference between the NPK-CARN and NPKA-CARN tumors, as all of the NPKA-CARN tumors contained a low but variable percentage of synaptophysin-positive neuroendocrine cells among total epithelial cells (0.7%, n=3), which were never observed in the NPK-CARN controls (0%, n=3) (Figure 6E, F). We also observed rare cells in all three NPKA-CARN tumors that expressed other neuroendocrine markers such as Chromogranin A, Foxa2, and Aurora kinase A (Figure 6E). Since the synaptophysin-postive cells co-expressed YFP (Figure 6E), we conclude that transformed AR-negative CARNs can give rise to neuroendocrine cells.

Discussion

Taken together, our analyses have defined specific roles for AR in regulating the progenitor properties of CARNs, and indicate that the intrinsic castration-resistance of CARNs is independent of AR function. We find that targeted deletion of AR does not affect the percentage of CARNs, their luminal marker expression, or their ability to generate basal cells during androgen-mediated regeneration. However, there are fewer luminal progeny from AR-deleted CARNs during regeneration *in vivo,* and there is a decreased efficiency of prostate duct formation by both AR-deleted CARNs and ADCA cells in renal grafts. Thus, AR deletion in CARNs may primarily affect the proliferation and/or survival of their luminal progeny *in vivo,* although an effect on CARNs themselves cannot be excluded.

Interestingly, our results suggest potential roles of the stroma in modulating the proliferation of CARNs and/or their luminal progeny. Notably, BrdU incorporation assays reveal a proliferation defect of AR-deleted CARNs during later stages of regeneration but not during early regeneration. One possible explanation is that AR activity may cell-autonomously regulate the proliferation of luminal progeny of CARNs; alternatively, however, stromal remodeling during later stages of regeneration may alter non-cell autonomous signals that regulate luminal proliferation. Furthermore, since ADCA cells do not display a growth defect in culture, their decreased efficiency of prostate duct formation in grafts is likely due to a non-cell-autonomous inhibitory effect from the stroma.

Our study has also yielded interesting insights into differences between CARNs and other luminal epithelial cells. While this manuscript was in preparation, another study also investigated the requirements of AR in CARNs, and reported that AR-deleted CARNs completely failed to generate progeny during regeneration (Xie et al., 2017). This apparent discrepancy may be partially explained by our observation that AR-deleted CARNs can still generate basal progeny, and by the failure of progeny from AR-deleted CARNs to proliferate at later stages of androgen-mediated regeneration. However, we concur that CARNs require AR function to generate viable

luminal progeny, which is not the case for most luminal cells during homeostasis or regeneration (Xie et al., 2017; Zhang et al., 2016a). Furthermore, the decreased proliferation of AR-deleted CARNs during regeneration contrasts with the transient increase in luminal proliferation observed after inducible AR deletion in the adult prostate epithelium, which is also a non-cell-autonomous effect mediated by the stroma (Zhang et al., 2016a). Together with our previous finding that CARNs display increased organoid formation efficiency relative to other luminal cells (Chua et al., 2014), these findings support the identification of CARNs as a distinct luminal population with stem/progenitor properties, and highlight the complexity of AR functions in the epithelial and stromal compartments.

In addition, we note that Xie and colleagues reported that *Pten* deletion in CARNs resulted in tumor formation after regeneration (Xie et al., 2017), unlike the absence of tumors that we observe in NPA-CARN mice. At present, the basis for this discrepancy remains unclear. Our finding that AR deletion results in failure of tumor formation following *Pten* inactivation could be due to differences between CARNs and bulk luminal cells and/or to differences due to *Pten* loss in the regressed versus hormonally-intact prostate epithelium. In principle, these possibilities could potentially be distinguished using inducible Cre-drivers to delete *Pten* in bulk luminal cells in regressed versus hormonally-intact mice.

Our findings on CARNs in mouse models may be of potential relevance for human prostate biology and cancer. Although CARNs are defined in the regressed prostate epithelium, and our *in vivo* studies involve manipulations performed after castration in mice, there is evidence that CARN-like cells exist in the human prostate from tissue-slice culture experiments (Zhao et al., 2010), as well as from analyses of prostate tumors after androgen-deprivation (Germann et al., 2012). However, it is less clear whether multipotent luminal progenitors can be identified in the context of the hormonally-intact human prostate. Previous lineage-reconstruction studies using patterns of mitochondrial DNA mutations have indicated the existence of multipotent epithelial progenitors (Blackwood et al., 2011; Gaisa et al., 2011), and

recent work has provided evidence for multipotent basal progenitors localized to the most proximal region of the prostate as well as more distally located unipotent luminal progenitors (Moad et al., 2017). Notably, *ex vivo* studies of human prostate organoids have demonstrated the existence of bipotential luminal progenitors (Karthaus et al., 2014). Thus, we believe that current data favor a general similarity of epithelial lineage relationships in the two species, suggesting that findings deduced from analyses of mice may be translatable to the human prostate.

The ability of CARNs to retain progenitor properties even in the absence of AR raises the possibility that CARNs represent a cell of origin for prostate cancers that are particularly susceptible to develop castration-resistance. Notably, under conditions of AR down-regulation, such as those that may occur during aging or inflammation, CARNs that lack tumor suppressors such as PTEN may represent a latent target for subsequent oncogenic events that can confer tumor growth, such as those activating the ERK MAP kinase pathway. Interestingly, our bioinformatic analyses of the ADCA cell line signature shows enrichment with castration-resistance signatures based on expression data from human prostate cancer patients (Best and Stanbrough signatures), consistent with increasing evidence supporting AR-independent mechanisms of castration-resistance (Beltran et al., 2014; Vlachostergios et al., 2017; Watson et al., 2015). In addition, the observed enrichment with the Beltran CRPC-NE signature suggests a similarity in gene expression programs with advanced cancers that lack AR activity, as neuroendocrine differentiation in prostate tumors is associated with loss of AR expression (Beltran et al., 2011). Notably, consistent with a role for AR loss in the emergence of neuroendocrine phenotypes, tumors in NPKA-CARN mice can display focal neuroendocrine differentiation, which has also been recently described in other mouse models of advanced prostate cancer (Ku et al., 2017; Zou et al., 2017).

In this regard, we note that the NP-CARN and NPK-CARN mice develop tumor phenotypes similar to those in NP and NPK mice, which have the same genotypes but whose tumors are induced by the *Nkx3.1*^{CreERT2} driver in hormonally-intact adult prostate (Aytes et al.,

2013; Floc'h et al., 2012). Interestingly, NP tumors are initially castration-sensitive (Floc'h et al., 2012), consistent with the inability of NPA-CARN mice to develop tumors, whereas NPK tumors are castration-resistant (Aytes et al., 2013), consistent with the phenotype of NPKA-CARN tumors. The molecular basis for this switch is currently unclear, but it is conceivable that it involves ETS family transcription factors, which are known to interact with AR to positively and negatively modulate its activity (Baena et al., 2013; Bose et al., 2017; Chen et al., 2013); interestingly, ETV4 is up-regulated in NPK tumors and may be involved in this switch (Aytes et al., 2013). However, the focal neuroendocrine differentiation observed in NPKA-CARN tumors suggests that oncogenic transformation of AR-deleted CARNs can also facilitate transdifferentiation of luminal cells to neuroendocrine fates, as we have demonstrated for a *Pten* and *Trp53* mutant mouse model (NPp53) after anti-androgen treatment (Zou et al., 2017).

Finally, since tumors initiated from CARNs following combined *Pten* deletion and *Kras* activation are at least partially independent of AR from their outset, it is conceivable that such tumors are intrinsically more resistant to second-generation anti-androgen therapies. Interestingly, recent studies have also identified distinct castration-resistant progenitors that express Bmi1 (CARBs) that are cells of origin for prostate cancer (Yoo et al., 2016). The development of targeted therapies directed at molecular features of CARNs and/or other castration-resistant luminal cells may therefore be relevant for successful combination with anti-androgen therapies.

Key Resources Table

Reagent type (species) or resource	Designation	Source or reference	Identifiers	Additional information
Strain (Mus musculus)	NOG	PMID: 15879151	NOD.Cg-*Prkdc*^{scid} *Il2rg*^{tm1Sug}/JicTac	Taconic
Strain (Mus musculus)	*Nkx3.1*^{CreERT2}	PMID: 19741607	*Nkx3-1*$^{tm4(CreERT2)Mms}$	established by Shen lab
Strain (Mus musculus)	*Pten*^{lox}	PMID: 11691952	C;129S4-*Pten*^{tm1Hwu}/J	JAX #004597
Strain (Mus musculus)	*Kras*$^{LSL-G12D}$	PMID: 11751630	B6.129-*Kras*^{tm4Tyj}/Nci	MMHCC #01XJ6
Strain (Mus musculus)	*AR*^{lox}	PMID: 14745012	B6N.129-*Ar*^{tm1Verh}/Cnrm	EMMA #02579
Strain (Mus musculus)	*R26R-YFP*	PMID: 11299042	B6.129X1-*Gt(ROSA)26Sor*$^{tm1(EYFP)Cos}$/J	JAX #006148
Cell line (Homo sapiens)	HPE-1	this work		Adherent cell line established from radical prostatectomy 23 tissue, sorted for EpCAM^{+}Ecad^{+} cells
Cell line (Homo sapiens)	HPE-2	this work		Adherent cell line established from radical prostatectomy 23 tissue, sorted for EpCAM^{+}Ecad^{+} cells
Cell line (Homo sapiens)	HPE-3	this work		Adherent cell line established from radical prostatectomy 24 tissue, sorted for EpCAM^{+}Ecad^{+} cells
Cell line (Homo sapiens)	HPE-4	this work		Adherent cell line established using radical prostatectomy 25 tissue
Cell line (Homo sapiens)	HPE-5	this work		Adherent cell line established from radical prostatectomy 25 tissue, sorted for EpCAM^{+}Ecad^{+} cells
Cell line (Homo sapiens)	HPE-6	this work		Adherent cell line established from radical prostatectomy 25 tissue, sorted for EpCAM^{+}Ecad^{+}Ngfr^{+} cells
Cell line (Homo sapiens)	HPE-7	this work		Adherent cell line established from radical prostatectomy 25 tissue, sorted for EpCAM^{+}Ecad^{+}Cd24^{+} cells
Cell line (Homo sapiens)	HPE-8	this work		Adherent cell line established from radical prostatectomy 26 tissue
Cell line (Homo sapiens)	HPE-9	this work		Adherent cell line established from radical prostatectomy 26 tissue, sorted for EpCAM^{+}Ecad^{+} cells
Cell line (Homo sapiens)	HPE-10	this work		Adherent cell line established from radical prostatectomy 26 tissue, sorted for EpCAM^{+}Ecad^{+}Cd24^{+} cells
Cell line (Homo sapiens)	HPE-11	this work		Adherent cell line established from radical prostatectomy 26 tissue, sorted for EpCAM^{+}Ecad^{+}Agr2^{+} cells

cell line (Homo sapiens)	HPE-12	this work		Adherent cell line established from radical prostatectomy 27 tissue
cell line (Homo sapiens)	HPE-13	this work		Adherent cell line established from radical prostatectomy 27 tissue; sorted for $EpCAM^{+}Ecad^{+}$ cells
cell line (Homo sapiens)	HPE-14	this work		Adherent cell line established from radical prostatectomy 27 tissue, sorted for $EpCAM^{+}Ecad^{+}Cd24^{+}$ cells
cell line (Mus musculus)	ADCA-1	this work		Adherent cell line established from single YFP^{+} cell isolated from castrated and tamoxifen-treated *Nkx3.1*$^{CreERT2/+}$*; Ar*$^{flox/Y}$*; R262R-YFP/+* mouse with deleted *Ar* (recombined) allele
cell line (Mus musculus)	ADCA-2	this work		Adherent cell line established from single YFP^{+} cell isolated from castrated and tamoxifen-treated *Nkx3.1*$^{CreERT2/+}$*; Ar*$^{flox/Y}$*; R262R-YFP/+* mouse with deleted *Ar* (recombined) allele
cell line (Mus musculus)	APCA-1	this work		Adherent cell line established from single YFP^{+} cell isolated from castrated and tamoxifen-treated *Nkx3.1*$^{CreERT2/+}$*; Ar*$^{flox/Y}$*; R262R-YFP/+* mouse with intact *Ar* (non-recombined) allele
cell line (Mus musculus)	APCA-2	this work		Adherent cell line established from single YFP^{+} cell isolated from castrated and tamoxifen-treated *Nkx3.1*$^{CreERT2/+}$*; Ar*$^{flox/Y}$*; R262R-YFP/+* mouse with intact *Ar* (non-recombined) allele
antibody	Androgen receptor (AR)	Sigma	A9853	
antibody	Cytokeratin 8 (CK8)	Developmental Studies Hybridoma Bank	TROMA-1	
antibody	Cytokeratin 18 (CK18)	Abcam	ab668	
antibody	Cytokeratin 5 (CK5)	Covance	SIG3475	
antibody	Cytokeratin 5 (CK5)	Covance	PRB-160P	
antibody	p63	Santa Cruz	sc-8431	
antibody	GFP	Abcam	ab13970	
antibody	GFP	Roche	11814460001	
antibody	BrdU	AbD Serotec MCA	2060	
antibody	Foxa1	Abcam	ab55178	

antibody	Ki67	eBiosciences	14-5698, clone SolA15	
antibody	Cleaved-caspase-3 (CC3)	BD Pharmingen	559565	
antibody	Prostate specific antigen (PSA)	Dako	M0750, clone ER-PR8	
antibody	Kras	Abcam	ab84573	
antibody	Synaptophysin (Syn)	BD Transduction Laboratories	611880	
antibody	Aurora A (Aurka)	Abcam	ab13824	
antibody	Chromogranin A (ChrA)	Abcam	ab15160	
antibody	Foxa2	Abnova	H00003170-M12	
antibody	AMACR	Zeta Corp	Z2001	
antibody	EpCAM	BioLegend	118214	
antibody	E-cadherin	eBiosciences	46-3249-82	
antibody	Nerve growth factor receptor (Ngfr)	BioLegend	345108	
antibody	Cd24	BioLegend	311008	
antibody	Anterior gradient 2 (Agr2)	Abcam	ab1139894	
antibody	EpCAM	BioLegend	324208	
sequence-based reagent	*Nkx3.1* wild-type primers	PMID: 19741607	DOI 10.1038/nature08361	
sequence-based reagent	*Nkx3.1*^{CreERT2} primers	PMID: 19741607	DOI 10.1038/nature08361	
sequence-based reagent	*CreER*^{T2} primers	PMID: 19741607	DOI 10.1038/nature08361	
sequence-based reagent	*R262R-YFP* primers	PMID: 11299042		
sequence-based reagent	*Pten*^{flox} primers	PMID: 11691952	DOI: 10.1126/science.1065518	
sequence-based reagent	*Pten* wild-type primers	PMID: 11691952	DOI: 10.1126/science.1065518	
sequence-based reagent	*Kras*$^{LSL-G12D}$ primers	PMID: 11751630	DOI:10.1101/gad.943001	
sequence-based reagent	*Kras* wild-type primers	PMID: 11751630	DOI:10.1101/gad.943001	
sequence-based reagent	*Ar*^{flox} primers	PMID: 14676301	DOI: 10.1084/jem.20031233	
sequence-based reagent	*Ar* wild-type primers	PMID: 14676301	DOI: 10.1084/jem.20031233	
sequence-based reagent	*Ar*^{flox} (recombined) primers	PMID: 14676301	DOI: 10.1084/jem.20031233	
sequence-based reagent	*Ar*^{flox} (not recombined) primers	PMID: 14676301	DOI: 10.1084/jem.20031233	
commercial assay or kit	Tyramide amplification	ThermoFisher Scientific	T20922	
commercial assay or kit	Tyramide amplification	ThermoFisher Scientific	T30953	
commercial assay or kit	Tyramide amplification	ThermoFisher Scientific	T30954	
commercial	Tyramide	ThermoFisher	T20926	

assay or kit	amplification	Scientific		
commercial assay or kit	Tyramide amplification	ThermoFisher Scientific	T20912	
commercial assay or kit	ABC Elite	Vector Labs	pk6101	
commercial assay or kit	Citrate-based antigen unmasking solution	Vector Labs	H3300	
commercial assay or kit	Tris-based antigen unmasking solution	Vector Labs	H3301	
commercial assay or kit	NovaRED	Vector Labs	SK3800	
commercial assay or kit	CellTiter-Glo 3D	Promega	G9681	
commercial assay or kit	MagMAX™-96 for Microarrays Total RNA Isolation Kit	Ambion	Am1839	Used the "no spin" protocol for RNA purification
commercial assay or kit	TruSeq Stranded mRNA library prep kit	Illumina	20020595	Library preparation was performed by the Columbia Genome Center using Illumina kits
chemical compound, drug	Tissue Tek OCT compound	VWR Scientific	25608-930	
chemical compound, drug	Glutamax	Invitrogen	35050061	
chemical compound, drug	Tamoxifen; TM	Sigma	T5648-5G	
chemical compound, drug	Gentamicin	Invitrogen	15750-060	
chemical compound, drug	Collagenase/hyaluronidase	STEMCELL Technologies	07912	
chemical compound, drug	Modified Hank's Balanced Salt Solution; HBSS	STEMCELL Technologies	37150	
chemical compound, drug	Dnase I	STEMCELL Technologies	07900	
chemical compound, drug	Y-27632 ROCK inhibitor	STEMCELL Technologies	72307	
chemical compound, drug	10x Earle's Balanced Salt Solution	ThermoFisher Scientific	14155063	
chemical compound, drug	Hepatocyte medium supplemented with epidermal growth factor (EGF)	Corning	355056	
chemical compound, drug	Matrigel	ThermoFisher Scientific	354234	
chemical compound, drug	0.25% trypsin-EDTA	STEMCELL Technologies	07901	
chemical compound, drug	FBS	ThermoFisher Scientific	12676029	
chemical compound, drug	DMEM/F12	ThermoFisher Scientific	11320033	
chemical compound, drug	BrdU	Sigma	B5002	
chemical compound, drug	Dispase	STEMCELL Technologies	07913	
chemical compound, drug	Dihydrotestosterone; DHT	Sigma	A8380	

software, algorithm	Real time analysis; RTA	Illumina	https://support.illumina.com/sequencing/sequencing_software/real-time_analysis_rta.html	Base calling using this software was performed by the Columbia Genome Center
software, algorithm	bcl2fastq2	Illumina	Ilumina: version 2.17	The sequencing data was trimmed and converted to fastq format by the Columbia Genome Center
software, algorithm	Spliced Transcripts Alignment to a Reference (STAR)	PMID: 23104886	Github: version 2.5.2b	Sequencing reads mapping to mouse genome (USCS/mm10) was performed by the Columbia Genome Center
software, algorithm	FeatureCounts	PMID: 24227677	subread.sourceforge.net version: v1.5.0-p3	Sequencing reads mapping to mouse genome (USCS/mm10) was performed by the Columbia Genome Center
software, algorithm	R-studio 0.99.902, R v3.3.0	The R Foundation for Statistical Computing, ISBN 3-900051-07-0	v3.3.0	R language for statistical computing was used for data analysis and visualization
software, algorithm	homoloGene	NCBI		
software, algorithm	Gene Set Enrichment Analysis	PMID: 16199517	DOI 10.1073/pnas.0506580102	GSEA was used to compares differential gene expression signatures
software, algorithm	Statistical Package for the Social Sciences; SPSS, Kolmogorov-Smirnov test, Arcsine transformation, Welch t-test, Fisher's Exact Test	IBM SPSS Statistics		
software, algorithm	Histological grading of mouse prostate phenotypes	PMID: 12163397	DOI 10.1016/S0002-9440(10)64228-9	
other	Mini-osmotic pump	Alzet	0000298	
other	40 μm cell strainer	Falcon	Fisher Scientific 352340	
other	96-well Primaria plate	Corning	Fisher Scientific 353872	
other	6-well Primaria plate	Corning	Fisher Scientific 353846	
other	96-well CELLSTAR plate	Sigma	M3587	
other	Lab-Tek Chamber Slide	Fisher Scientific	154534	

Materials and Methods

Mouse strains and genotyping

The *Nkx3.1*^{CreERT2} driver *(Nkx3-1*$^{tm4(cre/ERT2)Mms}$*)* has been previously described (Wang et al., 2009). Mice carrying the *R26R-YFP* (*B6.129X1-Gt(ROSA)26Sor*$^{tm1(EYFP)Cos}$*/J*) reporter (Srinivas et al., 2001) were obtained from the Jackson Laboratory Induced Mutant Resource. Mice carrying the conditional *Pten*^{flox} (B6.129S4-*Pten*^{tm1Hwu}*/J*) allele (Lesche et al., 2002) and the inducible *Kras*$^{lsl\text{-}G12D}$ (B6.129-*Kras*^{tm4Tyj}*/Nci*) allele (Jackson et al., 2001) were obtained from the National Cancer Institute Mouse Models of Human Cancer Consortium Repository. Mice with the conditional *Ar*^{flox} (*B6N.129-Ar*^{tm1Verh}*/Cnrm*) allele (De Gendt et al., 2004) was obtained from the European Mouse Mutant Archive. Animals were maintained on a congenic C57BL/6N background. Genotyping was performed using the primers listed in Supplementary file 1A. Primer sequences used for genotyping of *Ar* alleles were previously described (Yeh et al., 2003).

Mouse procedures

For lineage-marking and simultaneous deletion of *AR* in CARNs, *Nkx3.1*$^{CreERT2/+}$*; Ar*$^{flox/Y}$*; R26R-YFP/+* males were castrated at 8 weeks of age and allowed to regress for 4 weeks, followed by administration of tamoxifen (Sigma; 9 mg/40 g body weight in corn oil) by daily oral gavage for 4 consecutive days, and a chase period of 4 weeks. Administration of testosterone for prostate regeneration (Sigma; 25 mg /ml in 100% ethanol and diluted in PEG-400 to a final concentration of 7.5 mg/ml) was performed by subcutaneous implantation of mini-osmotic pumps (Alzet) that release testosterone solution at a rate of 1.875 μg/hour, which yields physiological levels of serum testosterone (Banach-Petrosky et al., 2007). For BrdU incorporation experiments, BrdU (Sigma; 100 mg/kg) was administered by intraperitoneal injection twice daily for four consecutive days, either from days 1 through 4 or from days 11 through 14 during androgen-mediated regeneration.

For cell of origin experiments, *Nkx3.1*$^{CreERT2/+}$*; Pten*$^{flox/flox}$*; Ar*$^{flox/Y}$*; R26R-YFP/+* and *Nkx3.1*$^{CreERT2/+}$*; Pten*$^{flox/flox}$*; Kras*$^{LSL-G12D/+}$*; Ar*$^{flox/Y}$*; R26R-YFP/+* mice as well as corresponding controls were castrated at 8 to 12 weeks of age. One month later, mice were administered tamoxifen, with a chase period of 3 months, followed by androgen-mediated regeneration for one month; mice were then euthanized for analysis. All animal experiments were performed according to protocols approved by the Institutional Animal Care and Use Committee at Columbia University Medical Center.

Benign human prostate specimens

Radical prostatectomy samples were obtained from consented patients under the auspices of an Institutional Review Board approved protocol at Columbia University Medical Center. Tissue from benign prostate regions was dissected and transported to the laboratory in DMEM/F12 (Gibco) supplemented with 5% FBS. Benign pathology was first determined by H&E-staining of snap-frozen sections, and subsequently confirmed by immunostaining of paraffin sections for p63 and AMACR.

Tissue acquisition, dissociation and isolation of prostate epithelial cells

Tissue dissociation and isolation were performed as previously described (Chua et al., 2014). In brief, mouse prostate tissue from all lobes was dissected in cold phosphate buffered saline (PBS) and minced with scissors. For human prostate specimens, tissue was cut into small pieces with scalpels, washed with PBS with 4 mg/ml Gentamicin (Gibco), and then minced with scissors. Both mouse and human prostate tissues were then incubated in DMEM/F12 (Gibco) supplemented with 5% FBS and 1:10 dilution of collagenase/hyaluronidase (STEMCELL Technologies) at 37°C for 3 hrs. Dissociated tissues were spun at 350 g for 5 min, and resuspended in ice-cold 0.25% trypsin-EDTA (STEMCELL Technologies), followed by incubation at 4°C for 1 hr. Trypsinization was stopped by addition of Modified Hank's Balanced Salt Solution (HBSS) (STEMCELL Technologies) supplemented with 2% FBS. After

centrifugation at 350 g, pelleted cells were resuspended with pre-warmed 5 mg/ml dispase (STEMCELL Technologies) supplemented with 1:10 dilution of 1 mg/ml DNase I (STEMCELL Technologies), triturated vigorously for 1 to 2 min, and diluted by addition of HBSS/2% FBS. Finally, the cell suspension was passed through a 40 μm cell strainer (Falcon).

Flow cytometry

For flow sorting of mouse prostate epithelial cells, cell suspensions were stained on ice for 25 min with fluorescent-tagged EpCAM (BioLegend #118214) antibody. For isolation of human prostate epithelial cells, we used fluorescent-tagged EpCAM (BioLegend #324208, specific for human) and E-cadherin (eBioscience #46-3249-82) antibodies. The stained cells were spun, and cell pellets washed with HBSS/2% FBS, followed by resuspension in HBSS/2% FBS with 10 μM Y-27632 (ROCK inhibitor; STEMCELL Technologies) and a 1:1,000 dilution of 0.5 mg/ml DAPI to exclude dead cells. Both side-scatter pulse width (SSC-W) vs. area (SSC-A) and forward side-scatter pulse area (FSC-A) vs. heights (FSC-H) were used to isolate single dissociated cells.

Adherent culture for mouse and human prostate epithelial cells

To establish cell lines from lineage-marked CARNs as well as benign prostate epithelial cells, we performed adherent culture in our prostate organoid medium (Chua et al., 2014), consisting of hepatocyte medium supplemented with 10 ng/ml epidermal growth factor (EGF) (Corning), 10 μM Y-27632 (STEMCELL Technologies), 1x glutamax (Gibco), 5% Matrigel (Corning), 5% charcoal-stripped FBS (Gibco) heat-inactivated at 55°C for 1 hr, and supplemented with either 100 nM or 1 nM DHT (Sigma) for mouse and human cells respectively. To derive APCA and ADCA lines, single YFP^{+} cells from castrated and tamoxifen-treated *Nkx3.1*$^{CreERT2/+}$*; Ar*$^{flox/Y}$*; R26R-YFP/+* mice were flow-sorted directly into 96-well Primaria plates (Corning), and were monitored daily to assess colony formation. Successful colonies were expanded and genotyped to assess the status of the *Ar*^{flox} allele. For derivation of

lines from benign human prostate epithelium, cells expressing either EpCAM and/or E-cadherin were plated into 6-well Primaria plates at a density of 100,000 cells/well.

Passaging of adherent cultures was performed by removal of accumulated Matrigel on surface of the cells by gentle washing. The cells were washed with cold PBS, treated with 0.25% trypsin for 5 minutes at 37°C, and mechanically dissociated. Medium was changed every 4 days. Adherent cells were frozen in media consisting of 80% FBS, 10% complete medium, and 10% DMSO. Each APCA and ADCA line has been propagated continuously for at least 8 passages.

Cell culture assays

To assess cell viability, APCA and ADCA lines were plated in 96-well Primaria plates at a density of 1,000 cells/well in the presence or absence of DHT. Cell viability was assayed at days 1, 2, 4 and 6 after plating using CellTiter-Glo 3D (Promega), with 5 technical replicates for each time point. In brief, CellTiter-Glo 3D reagent was thawed at 4°C and brought to room temperature prior to use. 100 μl of the reagent was added into each well containing 100 μl of medium. After shaking for 5-10 min, the mixture was then transferred to a 96-well CELLSTAR plate (Greiner), followed by incubation at room temperature for 10 min prior to measurement using a luminometer plate reader.

To assess colony formation, APCA and ADCA lines were plated in 6-well Primaria plates at a density of 500 cells/well and grown for 9 days. 3 technical replicates were performed for each line in the presence or absence of DHT. At day 10 after plating, wells were washed with PBS and fixed with 100% methanol for 5 min. The wells were then washed with PBS for 3 times before staining with filtered 0.1% crystal violet solution. After drying the plates, colonies were counted, with a colony defined as a cell cluster containing at least 50 cells.

Tissue recombination and renal grafting

For tissue recombination, 10 YFP^{+} cells from castrated and tamoxifen-treated *Nkx3.1*$^{CreERT2/+}$*; Ar*$^{flox/Y}$*; R26R-YFP/+* mice or control *Nkx3.1*$^{CreERT2/+}$*; R26R-YFP/+* mice were

combined with 250,000 dissociated rat urogenital mesenchyme cells from embryonic day 18.5 embryos, and resuspended in 15 μl of 9:1 collagen:setting buffer solution (10x Earle's Balanced Salt Solution (Life Technologies), 0.2 M $NaHCO_3$, and 50 mM NaOH). The recombinants were cultured overnight in DMEM with 10% FBS and 100 nM DHT, followed by grafting under the kidney capsules of male NOD.Cg-*Prkdc*^{scid} *Il2rg*^{tm1Sug}/JicTac (NOG) mice (Taconic). Renal grafts were harvested for analysis at 7-12 weeks after grafting. For the experiment involving APCA and ADCA lines, 100,000 cells were recombined with 250,000 rat urogenital mesenchyme cells, followed by grafting. At 6 weeks after grafting, some mice implanted with APCA cells were treated with tamoxifen to induce *Ar* deletion.

Grafts were harvested for analysis after 12 weeks of growth and analyzed in paraffin sections for the presence of ducts expressing YFP. (Note that ducts can also be formed by YFP^- cells that are derived from contaminating rat urogenital epithelium due to incomplete separation from the urogenital mesenchyme.) Graft efficiency was calculated on the basis of the presence of YFP^+ ducts in the grafts using control CARNs and on the presence of YFP^+AR^- ducts in the grafts using AR-deleted CARNs.

Histology and immunostaining

For cryosections, tissues were fixed in 4% paraformaldehyde in PBS at 4°C overnight, placed in 30% sucrose in PBS overnight, and transferred to 1:1 30% sucrose in PBS and OCT (Tissue-Tek) solution for at least 4 hrs prior to embedding in OCT. For paraffin sections, tissues were fixed in 10% formalin for 1 to 2 days, depending on size of tissue, prior to processing and embedding. Hematoxylin-eosin staining was performed using standard protocols. For immunostaining, sections underwent antigen-retrieval by heating in citrate acid-based or tris-based antigen unmasking solution (Vector Labs) for 45 min. Primary antibodies were applied to sections and incubated at 4°C overnight in a humidified chamber. Alexa Fluors (Life Technologies) were used as secondary antibodies. In some cases, tyramide amplification (Life Technologies) or ABC Elite (Vector Labs) kits together with HRP-conjugated or biotinylated

secondary antibodies and NovaRed kit were used for signal detection. For immunofluorescent staining of cells, 5,000 adherent cells/well were seeded on a 8-well Lab-Tek Chamber Slide (Nunc), grown for 4-8 days, and fixed with 4% paraformaldehyde for 10 min. After washing the slides with 3 changes of PBS, immunostaining was performed as above without antigen retrieval. Details of antibodies used are provided in Supplementary file 1B.

Histological grading of mouse prostate phenotypes was performed according to (Park et al., 2002). For lineage-tracing experiments, quantitation of marker staining was performed by manual counting of cells from confocal images taken with a 40x objective.

RNA sequencing and bioinformatic analysis

For RNA preparation, APCA and ADCA cell lines at passage 5 or 6 were grown to approximately 70-80% confluency in Primaria 6-well plates in the presence of DHT, and lysed in Trizol. Total RNA extraction was performed using the "No Spin" method of the MagMAX-96 for Microarrays kit (Ambion). Library preparation and RNA sequencing was performed by the Columbia Genome Center using their standard pipeline. In brief, mRNA was enriched by poly-A pull-down, and library preparation was performed using an Illumina TruSeq RNA prep kit. Libraries were pooled and sequenced using an Illumina HiSeq2500 instrument, yielding approximately 30 million single-ended 100 bp reads per sample. RTA (Illumina) was used for base calling and bcl2fastq2 (version 2.17) for conversion of BCL to fastq format, coupled with adaptor trimming. Reads were mapped to the mouse genome (UCSC/mm10) using STAR (2.5.2b) and FeatureCounts (v1.5.0-p3).

RNA-seq data raw counts were normalized and the variance was stabilized using DESeq2 package (Bioconductor) in R-studio 0.99.902, R v3.3.0 (The R Foundation for Statistical Computing, ISBN 3-900051-07-0). Differential gene expression signatures were defined as a list of genes ranked by their differential expression between any two phenotypes of interest (*e.g.*, APCA versus ADCA lines; CRPC-NE versus CRPC, *etc*.), estimated using a 2-sample 2-tailed

Welch t-test (for $n \geq 3$) or fold-change (for $n < 3$). For comparison of a mouse gene signature with a human gene signature, mouse genes were mapped to their corresponding human orthologs based on the homoloGene database (NCBI). Signatures were compared using Gene Set Enrichment Analysis (GSEA) (Subramanian et al., 2005), with the significance of enrichment estimated using 1,000 gene permutations. Pathway enrichment analysis was performed using the C2 database, which includes pathways from REACTOME (Fabregat et al., 2016), KEGG (Ogata et al., 1999), and BioCarta (http://www.biocarta.com/genes/allpathways.asp). Expression data are deposited in the Gene Expression Omnibus database under GSE99233.

Statistical analyses

Statistical analysis was performed using the Statistical Package for the Social Sciences (SPSS). Data distribution was assessed by the Kolmogorov-Smirnov test. Arcsine transformation was performed on data with non-normal distribution. 2-sample 2-tail Welch t-test or Fisher's Exact Test was performed for comparison between 2 independent groups as appropriate. No statistical methods were used to pre-determine sample size, and experiments were not randomized; investigators were not blinded to allocation during experiments and outcome assessment.

Acknowledgements

We thank Robert Cardiff for advice on histology and Cory Abate-Shen, Laura Crowley, Maximilian Marhold, Maho Shibata, and Roxanne Toivanen for insightful discussions and comments on the manuscript. Our studies used the CCTI Flow Cytometry Core (supported in part by the Office of the Director, National Institutes of Health under awards S10RR027050), and the HICCC Molecular Pathology Shared Resource. This work was supported by post-doctoral fellowships from the DOD Prostate Cancer Research Program (C.W.C., B.I.L.), by a Rutgers SHP Dean's Research Intramural grant (A.M.), and by grants from the Prostate Cancer Foundation (M.M.S.) and the National Institutes of Health (M.M.S.).

Competing interests

The authors declare that they have no financial or non-financial competing interests.

References

Aytes, A., Mitrofanova, A., Kinkade, C.W., Lefebvre, C., Lei, M., Phelan, V., LeKaye, H.C., Koutcher, J.A., Cardiff, R.D., Califano, A., Shen, M.M., and Abate-Shen, C. (2013). ETV4 promotes metastasis in response to activation of PI3-kinase and Ras signaling in a mouse model of advanced prostate cancer. Proc Natl Acad Sci U S A *110*, E3506-3515. 10.1073/pnas.1303558110.

Baena, E., Shao, Z., Linn, D.E., Glass, K., Hamblen, M.J., Fujiwara, Y., Kim, J., Nguyen, M., Zhang, X., Godinho, F.J., Bronson, R.T., Mucci, L.A., Loda, M., Yuan, G.C., Orkin, S.H., and Li, Z. (2013). ETV1 directs androgen metabolism and confers aggressive prostate cancer in targeted mice and patients. Genes Dev *27*, 683-698. 10.1101/gad.211011.112.

Banach-Petrosky, W., Jessen, W.J., Ouyang, X., Gao, H., Rao, J., Quinn, J., Aronow, B.J., and Abate-Shen, C. (2007). Prolonged exposure to reduced levels of androgen accelerates prostate cancer progression in Nkx3.1; Pten mutant mice. Cancer Res *67*, 9089-9096.

Beltran, H., Prandi, D., Mosquera, J.M., Benelli, M., Puca, L., Cyrta, J., Marotz, C., Giannopoulou, E., Chakravarthi, B.V., Varambally, S., Tomlins, S.A., Nanus, D.M., Tagawa, S.T., Van Allen, E.M., Elemento, O., Sboner, A., Garraway, L.A., Rubin, M.A., and Demichelis, F. (2016). Divergent clonal evolution of castration-resistant neuroendocrine prostate cancer. Nat Med *22*, 298-305. 10.1038/nm.4045.

Beltran, H., Rickman, D.S., Park, K., Chae, S.S., Sboner, A., MacDonald, T.Y., Wang, Y., Sheikh, K.L., Terry, S., Tagawa, S.T., Dhir, R., Nelson, J.B., de la Taille, A., Allory, Y., Gerstein, M.B., Perner, S., Pienta, K.J., Chinnaiyan, A.M., Wang, Y., Collins, C.C., Gleave, M.E., Demichelis, F., Nanus, D.M., and Rubin, M.A. (2011). Molecular characterization of neuroendocrine prostate cancer and identification of new drug targets. Cancer Discov *1*, 487-495. 10.1158/2159-8290.CD-11-0130.

563 Beltran, H., Tomlins, S., Aparicio, A., Arora, V., Rickman, D., Ayala, G., Huang, J., True, L.,
564 Gleave, M.E., Soule, H., Logothetis, C., and Rubin, M.A. (2014). Aggressive variants of
565 castration-resistant prostate cancer. Clin Cancer Res *20*, 2846-2850. 10.1158/1078-
566 0432.CCR-13-3309.

567 Best, C.J., Gillespie, J.W., Yi, Y., Chandramouli, G.V., Perlmutter, M.A., Gathright, Y.,
568 Erickson, H.S., Georgevich, L., Tangrea, M.A., Duray, P.H., Gonzalez, S., Velasco, A.,
569 Linehan, W.M., Matusik, R.J., Price, D.K., Figg, W.D., Emmert-Buck, M.R., and
570 Chuaqui, R.F. (2005). Molecular alterations in primary prostate cancer after androgen
571 ablation therapy. Clin Cancer Res *11*, 6823-6834. 10.1158/1078-0432.CCR-05-0585.

572 Blackwood, J.K., Williamson, S.C., Greaves, L.C., Wilson, L., Rigas, A.C., Sandher, R.,
573 Pickard, R.S., Robson, C.N., Turnbull, D.M., Taylor, R.W., and Heer, R. (2011). In situ
574 lineage tracking of human prostatic epithelial stem cell fate reveals a common clonal
575 origin for basal and luminal cells. J Pathol *225*, 181-188. 10.1002/path.2965.

576 Blanpain, C. (2013). Tracing the cellular origin of cancer. Nat Cell Biol *15*, 126-134.
577 10.1038/ncb2657.

578 Bose, R., Karthaus, W.R., Armenia, J., Abida, W., Iaquinta, P.J., Zhang, Z., Wongvipat, J.,
579 Wasmuth, E.V., Shah, N., Sullivan, P.S., Doran, M.G., Wang, P., Patruno, A., Zhao, Y.,
580 International, S.U.C.P.C.F.P.C.D.T., Zheng, D., Schultz, N., and Sawyers, C.L. (2017).
581 ERF mutations reveal a balance of ETS factors controlling prostate oncogenesis. Nature
582 *546*, 671-675. 10.1038/nature22820.

583 Chen, Y., Chi, P., Rockowitz, S., Iaquinta, P.J., Shamu, T., Shukla, S., Gao, D., Sirota, I., Carver,
584 B.S., Wongvipat, J., Scher, H.I., Zheng, D., and Sawyers, C.L. (2013). ETS factors
585 reprogram the androgen receptor cistrome and prime prostate tumorigenesis in response
586 to PTEN loss. Nat Med *19*, 1023-1029. 10.1038/nm.3216.

587 Choi, N., Zhang, B., Zhang, L., Ittmann, M., and Xin, L. (2012). Adult murine prostate basal and
588 luminal cells are self-sustained lineages that can both serve as targets for prostate cancer
589 initiation. Cancer Cell *21*, 253-265. 10.1016/j.ccr.2012.01.005.

590 Chua, C.W., Shibata, M., Lei, M., Toivanen, R., Barlow, L.J., Bergren, S.K., Badani, K.K.,
591 McKiernan, J.M., Benson, M.C., Hibshoosh, H., and Shen, M.M. (2014). Single luminal
592 epithelial progenitors can generate prostate organoids in culture. Nat Cell Biol *16*, 951-
593 961. 10.1038/ncb3047.

594 Cunha, G.R., Ricke, W., Thomson, A., Marker, P.C., Risbridger, G., Hayward, S.W., Wang,
595 Y.Z., Donjacour, A.A., and Kurita, T. (2004). Hormonal, cellular, and molecular
596 regulation of normal and neoplastic prostatic development. J Steroid Biochem Mol Biol
597 *92*, 221-236. 10.1016/j.jsbmb.2004.10.017.

598 De Gendt, K., Swinnen, J.V., Saunders, P.T., Schoonjans, L., Dewerchin, M., Devos, A., Tan,
599 K., Atanassova, N., Claessens, F., Lecureuil, C., Heyns, W., Carmeliet, P., Guillou, F.,
600 Sharpe, R.M., and Verhoeven, G. (2004). A Sertoli cell-selective knockout of the
601 androgen receptor causes spermatogenic arrest in meiosis. Proc Natl Acad Sci USA *101*,
602 1327-1332. 10.1073/pnas.0308114100.

603 Fabregat, A., Sidiropoulos, K., Garapati, P., Gillespie, M., Hausmann, K., Haw, R., Jassal, B.,
604 Jupe, S., Korninger, F., McKay, S., Matthews, L., May, B., Milacic, M., Rothfels, K.,
605 Shamovsky, V., Webber, M., Weiser, J., Williams, M., Wu, G., Stein, L., Hermjakob, H.,
606 and D'Eustachio, P. (2016). The Reactome pathway Knowledgebase. Nucleic Acids Res
607 *44*, D481-487. 10.1093/nar/gkv1351.

608 Floc'h, N., Kinkade, C.W., Kobayashi, T., Aytes, A., Lefebvre, C., Mitrofanova, A., Cardiff,
609 R.D., Califano, A., Shen, M.M., and Abate-Shen, C. (2012). Dual targeting of the
610 Akt/mTOR signaling pathway inhibits castration-resistant prostate cancer in a genetically

611 engineered mouse model. Cancer Res *72*, 4483-4493. 10.1158/0008-5472.CAN-12-
612 0283.

613 Gaisa, N.T., Graham, T.A., McDonald, S.A., Poulsom, R., Heidenreich, A., Jakse, G., Knuechel,
614 R., and Wright, N.A. (2011). Clonal architecture of human prostatic epithelium in benign
615 and malignant conditions. J Pathol *225*, 172-180. 10.1002/path.2959.

616 Gao, N., Zhang, J., Rao, M.A., Case, T.C., Mirosevich, J., Wang, Y., Jin, R., Gupta, A., Rennie,
617 P.S., and Matusik, R.J. (2003). The role of hepatocyte nuclear factor-3 alpha (Forkhead
618 Box A1) and androgen receptor in transcriptional regulation of prostatic genes. Mol
619 Endocrinol *17*, 1484-1507. 10.1210/me.2003-0020.

620 Germann, M., Wetterwald, A., Guzman-Ramirez, N., van der Pluijm, G., Culig, Z., Cecchini,
621 M.G., Williams, E.D., and Thalmann, G.N. (2012). Stem-like cells with luminal
622 progenitor phenotype survive castration in human prostate cancer. Stem Cells *30*, 1076-
623 1086. 10.1002/stem.1087.

624 Goldstein, A.S., Lawson, D.A., Cheng, D., Sun, W., Garraway, I.P., and Witte, O.N. (2008).
625 Trop2 identifies a subpopulation of murine and human prostate basal cells with stem cell
626 characteristics. Proc Natl Acad Sci USA *105*, 20882-20887. 10.1073/pnas.0811411106.

627 Gurel, B., Iwata, T., Koh, C.M., Jenkins, R.B., Lan, F., Van Dang, C., Hicks, J.L., Morgan, J.,
628 Cornish, T.C., Sutcliffe, S., Isaacs, W.B., Luo, J., and De Marzo, A.M. (2008). Nuclear
629 MYC protein overexpression is an early alteration in human prostate carcinogenesis. Mod
630 Pathol *21*, 1156-1167. 10.1038/modpathol.2008.111.

631 He, H.H., Meyer, C.A., Shin, H., Bailey, S.T., Wei, G., Wang, Q., Zhang, Y., Xu, K., Ni, M.,
632 Lupien, M., Mieczkowski, P., Lieb, J.D., Zhao, K., Brown, M., and Liu, X.S. (2010).
633 Nucleosome dynamics define transcriptional enhancers. Nat Genet *42*, 343-347.
634 10.1038/ng.545.

635 Hofner, T., Eisen, C., Klein, C., Rigo-Watermeier, T., Goeppinger, S.M., Jauch, A., Schoell, B.,
636 Vogel, V., Noll, E., Weichert, W., Baccelli, I., Schillert, A., Wagner, S., Pahernik, S.,
637 Sprick, M.R., and Trumpp, A. (2015). Defined conditions for the isolation and expansion
638 of basal prostate progenitor cells of mouse and human origin. Stem Cell Reports *4*, 503-
639 518. 10.1016/j.stemcr.2015.01.015.

640 Jackson, E.L., Willis, N., Mercer, K., Bronson, R.T., Crowley, D., Montoya, R., Jacks, T., and
641 Tuveson, D.A. (2001). Analysis of lung tumor initiation and progression using
642 conditional expression of oncogenic K-ras. Genes Dev *15*, 3243-3248.

643 Karthaus, W.R., Iaquinta, P.J., Drost, J., Gracanin, A., van Boxtel, R., Wongvipat, J., Dowling,
644 C.M., Gao, D., Begthel, H., Sachs, N., Vries, R.G., Cuppen, E., Chen, Y., Sawyers, C.L.,
645 and Clevers, H.C. (2014). Identification of multipotent luminal progenitor cells in human
646 prostate organoid cultures. Cell *159*, 163-175. 10.1016/j.cell.2014.08.017.

647 Ku, S.Y., Rosario, S., Wang, Y., Mu, P., Seshadri, M., Goodrich, Z.W., Goodrich, M.M., Labbe,
648 D.P., Gomez, E.C., Wang, J., Long, H.W., Xu, B., Brown, M., Loda, M., Sawyers, C.L.,
649 Ellis, L., and Goodrich, D.W. (2017). Rb1 and Trp53 cooperate to suppress prostate
650 cancer lineage plasticity, metastasis, and antiandrogen resistance. Science *355*, 78-83.
651 10.1126/science.aah4199.

652 Kwon, O.J., Zhang, L., Ittmann, M.M., and Xin, L. (2014). Prostatic inflammation enhances
653 basal-to-luminal differentiation and accelerates initiation of prostate cancer with a basal
654 cell origin. Proc Natl Acad Sci USA *111*, E592-600. 10.1073/pnas.1318157111.

655 Kwon, O.J., Zhang, L., and Xin, L. (2016). Stem Cell Antigen-1 identifies a distinct androgen-
656 independent murine prostatic luminal cell lineage with bipotent potential. Stem Cells *34*,
657 191-202. 10.1002/stem.2217.

Lawson, D.A., Xin, L., Lukacs, R.U., Cheng, D., and Witte, O.N. (2007). Isolation and functional characterization of murine prostate stem cells. Proc Natl Acad Sci USA *104*, 181-186. 10.1073/pnas.0609684104.

Lee, S.H., and Shen, M.M. (2015). Cell types of origin for prostate cancer. Curr Opin Cell Biol *37*, 35-41. 10.1016/j.ceb.2015.10.002.

Lee, S.O., Tian, J., Huang, C.K., Ma, Z., Lai, K.P., Hsiao, H., Jiang, M., Yeh, S., and Chang, C. (2012). Suppressor role of androgen receptor in proliferation of prostate basal epithelial and progenitor cells. J Endocrinol *213*, 173-182. 10.1530/JOE-11-0474.

Lesche, R., Groszer, M., Gao, J., Wang, Y., Messing, A., Sun, H., Liu, X., and Wu, H. (2002). Cre/loxP-mediated inactivation of the murine Pten tumor suppressor gene. Genesis *32*, 148-149.

Liu, J., Pascal, L.E., Isharwal, S., Metzger, D., Ramos Garcia, R., Pilch, J., Kasper, S., Williams, K., Basse, P.H., Nelson, J.B., Chambon, P., and Wang, Z. (2011). Regenerated luminal epithelial cells are derived from preexisting luminal epithelial cells in adult mouse prostate. Mol Endocrinol *25*, 1849-1857. 10.1210/me.2011-1081.

Lu, T.L., Huang, Y.F., You, L.R., Chao, N.C., Su, F.Y., Chang, J.L., and Chen, C.M. (2013). Conditionally ablated Pten in prostate basal cells promotes basal-to-luminal differentiation and causes invasive prostate cancer in mice. Am J Pathol *182*, 975-991. 10.1016/j.ajpath.2012.11.025.

Meeker, A.K., Hicks, J.L., Platz, E.A., March, G.E., Bennett, C.J., Delannoy, M.J., and De Marzo, A.M. (2002). Telomere shortening is an early somatic DNA alteration in human prostate tumorigenesis. Cancer Res *62*, 6405-6409.

Mirosevich, J., Bentel, J.M., Zeps, N., Redmond, S.L., D'Antuono, M.F., and Dawkins, H.J. (1999). Androgen receptor expression of proliferating basal and luminal cells in adult murine ventral prostate. J Endocrinol *162*, 341-350.

683 Moad, M., Hannezo, E., Buczacki, S.J., Wilson, L., El-Sherif, A., Sims, D., Pickard, R., Wright,
684 N.A., Williamson, S.C., Turnbull, D.M., Taylor, R.W., Greaves, L., Robson, C.N.,
685 Simons, B.D., and Heer, R. (2017). Multipotent basal stem cells, maintained in localized
686 proximal niches, support directed long-ranging epithelial flows in human prostates. Cell
687 Rep *20*, 1609-1622. 10.1016/j.celrep.2017.07.061.

688 Mu, P., Zhang, Z., Benelli, M., Karthaus, W.R., Hoover, E., Chen, C.C., Wongvipat, J., Ku, S.Y.,
689 Gao, D., Cao, Z., Shah, N., Adams, E.J., Abida, W., Watson, P.A., Prandi, D., Huang,
690 C.H., de Stanchina, E., Lowe, S.W., Ellis, L., Beltran, H., Rubin, M.A., Goodrich, D.W.,
691 Demichelis, F., and Sawyers, C.L. (2017). SOX2 promotes lineage plasticity and
692 antiandrogen resistance in TP53- and RB1-deficient prostate cancer. Science *355*, 84-88.
693 10.1126/science.aah4307.

694 Ogata, H., Goto, S., Sato, K., Fujibuchi, W., Bono, H., and Kanehisa, M. (1999). KEGG: Kyoto
695 Encyclopedia of Genes and Genomes. Nucleic Acids Res *27*, 29-34.

696 Park, J.H., Walls, J.E., Galvez, J.J., Kim, M., Abate-Shen, C., Shen, M.M., and Cardiff, R.D.
697 (2002). Prostatic intraepithelial neoplasia in genetically engineered mice. Am J Pathol
698 *161*, 727-735.

699 Rycaj, K., and Tang, D.G. (2015). Cell-of-origin of cancer versus cancer stem cells: assays and
700 interpretations. Cancer Res *75*, 4003-4011. 10.1158/0008-5472.CAN-15-0798.

701 Shen, M.M., and Abate-Shen, C. (2010). Molecular genetics of prostate cancer: new prospects
702 for old challenges. Genes Dev *24*, 1967-2000. 10.1101/gad.1965810.

703 Shibata, M., and Shen, M.M. (2013). The roots of cancer: stem cells and the basis for tumor
704 heterogeneity. Bioessays *35*, 253-260. 10.1002/bies.201200101.

705 Srinivas, S., Watanabe, T., Lin, C.S., William, C.M., Tanabe, Y., Jessell, T.M., and Costantini,
706 F. (2001). Cre reporter strains produced by targeted insertion of EYFP and ECFP into the
707 ROSA26 locus. BMC Dev Biol *1*, 4.

Stanbrough, M., Bubley, G.J., Ross, K., Golub, T.R., Rubin, M.A., Penning, T.M., Febbo, P.G., and Balk, S.P. (2006). Increased expression of genes converting adrenal androgens to testosterone in androgen-independent prostate cancer. Cancer Res *66*, 2815-2825.

Subramanian, A., Tamayo, P., Mootha, V.K., Mukherjee, S., Ebert, B.L., Gillette, M.A., Paulovich, A., Pomeroy, S.L., Golub, T.R., Lander, E.S., and Mesirov, J.P. (2005). Gene set enrichment analysis: a knowledge-based approach for interpreting genome-wide expression profiles. Proc Natl Acad Sci U S A *102*, 15545-15550. 10.1073/pnas.0506580102.

Talos, F., Mitrofanova, A., Bergren, S.K., Califano, A., and Shen, M.M. (2017). A computational systems approach identifies synergistic specification genes that facilitate lineage conversion to prostate tissue. Nat Commun *8*, 14662. 10.1038/ncomms14662.

Toivanen, R., Mohan, A., and Shen, M.M. (2016). Basal progenitors contribute to repair of the prostate epithelium following induced luminal anoikis. Stem Cell Reports *6*, 660-667. 10.1016/j.stemcr.2016.03.007.

Toivanen, R., and Shen, M.M. (2017). Prostate organogenesis: tissue induction, hormonal regulation and cell type specification. Development *144*, 1382-1398. 10.1242/dev.148270.

Visvader, J.E. (2011). Cells of origin in cancer. Nature *469*, 314-322. 10.1038/nature09781.

Vlachostergios, P.J., Puca, L., and Beltran, H. (2017). Emerging variants of castration-resistant prostate cancer. Curr Oncol Rep *19*, 32. 10.1007/s11912-017-0593-6.

Wang, X., Kruithof-de Julio, M., Economides, K.D., Walker, D., Yu, H.L., Halili, M.V., Hu, Y.P., Price, S.M., Abate-Shen, C., and Shen, M.M. (2009). A luminal epithelial stem cell that is a cell of origin for prostate cancer. Nature *461*, 495-500. 10.1038/nature08361.

Wang, Z.A., Mitrofanova, A., Bergren, S.K., Abate-Shen, C., Cardiff, R.D., Califano, A., and Shen, M.M. (2013). Lineage analysis of basal epithelial cells reveals their unexpected

plasticity and supports a cell-of-origin model for prostate cancer heterogeneity. Nat Cell Biol *15*, 274-283. 10.1038/ncb2697.

Wang, Z.A., and Shen, M.M. (2011). Revisiting the concept of cancer stem cells in prostate cancer. Oncogene *30*, 1261-1271. 10.1038/onc.2010.530.

Wang, Z.A., Toivanen, R., Bergren, S.K., Chambon, P., and Shen, M.M. (2014). Luminal cells are favored as the cell of origin for prostate cancer. Cell Rep *8*, 1339-1346. 10.1016/j.celrep.2014.08.002.

Watson, P.A., Arora, V.K., and Sawyers, C.L. (2015). Emerging mechanisms of resistance to androgen receptor inhibitors in prostate cancer. Nat Rev Cancer *15*, 701-711. 10.1038/nrc4016.

Wu, C.T., Altuwaijri, S., Ricke, W.A., Huang, S.P., Yeh, S., Zhang, C., Niu, Y., Tsai, M.Y., and Chang, C. (2007). Increased prostate cell proliferation and loss of cell differentiation in mice lacking prostate epithelial androgen receptor. Proc Natl Acad Sci U S A *104*, 12679-12684. 10.1073/pnas.0704940104.

Xie, Q., Liu, Y., Cai, T., Horton, C., Stefanson, J., and Wang, Z.A. (2017). Dissecting cell-type-specific roles of androgen receptor in prostate homeostasis and regeneration through lineage tracing. Nat Commun *8*, 14284. 10.1038/ncomms14284.

Xin, L. (2013). Cells of origin for cancer: an updated view from prostate cancer. Oncogene *32*, 3655-3663. 10.1038/onc.2012.541.

Yeh, S., Hu, Y.C., Wang, P.H., Xie, C., Xu, Q., Tsai, M.Y., Dong, Z., Wang, R.S., Lee, T.H., and Chang, C. (2003). Abnormal mammary gland development and growth retardation in female mice and MCF7 breast cancer cells lacking androgen receptor. J Exp Med *198*, 1899-1908. 10.1084/jem.20031233.

Yoo, Y.A., Roh, M., Naseem, A.F., Lysy, B., Desouki, M.M., Unno, K., and Abdulkadir, S.A. (2016). Bmi1 marks distinct castration-resistant luminal progenitor cells competent for

prostate regeneration and tumour initiation. Nat Commun *7*, 12943. 10.1038/ncomms12943.

Zhang, B., Kwon, O.J., Henry, G., Malewska, A., Wei, X., Zhang, L., Brinkley, W., Zhang, Y., Castro, P.D., Titus, M., Chen, R., Sayeeduddin, M., Raj, G.V., Mauck, R., Roehrborn, C., Creighton, C.J., Strand, D.W., Ittmann, M.M., and Xin, L. (2016a). Non-cell-autonomous regulation of prostate epithelial homeostasis by androgen receptor. Mol Cell *63*, 976-989. 10.1016/j.molcel.2016.07.025.

Zhang, D., Park, D., Zhong, Y., Lu, Y., Rycaj, K., Gong, S., Chen, X., Liu, X., Chao, H.P., Whitney, P., Calhoun-Davis, T., Takata, Y., Shen, J., Iyer, V.R., and Tang, D.G. (2016b). Stem cell and neurogenic gene-expression profiles link prostate basal cells to aggressive prostate cancer. Nat Commun *7*, 10798. 10.1038/ncomms10798.

Zhao, H., Nolley, R., Chen, Z., and Peehl, D.M. (2010). Tissue slice grafts: an in vivo model of human prostate androgen signaling. Am J Pathol *177*, 229-239. ajpath.2010.090821

Zou, M., Toivanen, R., Mitrofanova, A., Floc'h, N., Hayati, S., Sun, Y., Le Magnen, C., Chester, D., Mostaghel, E.A., Califano, A., Rubin, M.A., Shen, M.M., and Abate-Shen, C. (2017). Transdifferentiation as a mechanism of treatment resistance in a mouse model of castration-resistant prostate cancer. Cancer Discov. 10.1158/2159-8290.CD-16-1174.

Figure Legends

Figure 1. CARNs remain luminal after AR deletion. (**A**) Time course for lineage-marking of CARNs and inducible *AR* deletion using castrated and tamoxifen-treated control *Nkx3.1*$^{CreERT2/+}$*; R26R-YFP/+* mice and *Nkx3.1*$^{CreERT2/+}$*;* *Ar*$^{flox/Y}$*; R26R-YFP/+* mice. (**B**) FACS analyses of lineage-marked YFP$^+$ cells in total EpCAM$^+$ epithelial cells. (**C**) Percentage of YFP$^+$ cells among total epithelial cells in castrated and tamoxifen-induced *Nkx3.1*$^{CreERT2/+}$*; R26R-YFP/+* controls and *Nkx3.1*$^{CreERT2/+}$*;* *Ar*$^{flox/Y}$*; R26R-YFP/+* mice. Error bars represent one standard deviation; the difference between groups is not significant (p=0.51, independent t-test). (**D**) Expression of AR, luminal markers (CK8 and CK18), and basal markers (CK5 and p63) in lineage-marked CARNs (top) and *AR*-deleted CARNs (bottom). Note that all lineage-marked cells express luminal but not basal markers (arrows). Scale bars in **D** correspond to 50 μm.

Figure 1 – source data. Quantitation of CARNs and AR-deleted CARNs *in vivo*.

Figure 2. AR-deleted CARNs fail to generate lineage-marked cell clusters but remain bipotential during androgen-mediated regeneration. (**A**) Time course for lineage-marking and androgen-mediated regeneration. (**B**) Percentage of single YFP$^+$ cells or YFP$^+$ clusters of 2 cells, 3-4 cells, and > 4-cells at 4, 7, 14, and 28 days of androgen-mediated regeneration. This analysis does not include YFP$^+$AR$^+$ cells that failed to undergo AR deletion in the experimental mice; full quantitation of all cell populations is provided in Figure 2 source data 1. (**C**) YFP$^+$ cells (arrows) in prostates of mice with lineage-marked CARNs (top) and AR-deleted CARNs (bottom) at days 4, 7, 14 and 28 days during androgen-mediated regeneration. (**D**) Identification of basal YFP$^+$ cells (arrows) as progeny of CARNs (top) or *AR*-deleted CARNs (bottom). Scale bars in **C** and **D** correspond to 50 μm.

Figure 2 – source data. Quantitation of YFP$^+$ cells during regeneration.

Figure 3. AR-deleted CARNs and/or their progeny have defects in proliferation during regeneration and in renal grafts. (**A**,**B**) Time course of BrdU incorporation during androgen-mediated regeneration of castrated and tamoxifen-treated control *Nkx3.1$^{CreERT2/+}$; R26R-YFP/+* mice and *Nkx3.1$^{CreERT2/+}$; Ar$^{flox/Y}$; R26R-YFP/+* mice. BrdU injections were performed during either days 1 through 4 (**A**) or days 11 through 14 (**B**), followed by analysis at 28 days. (**C**) Identification of BrdU^{+}YFP^{+} cells (arrows) in control (top) and AR-deleted (bottom) prostate tissue after administration of BrdU during early stages of regeneration. (**D**) YFP-positive cells in control prostate tumors (top) can incorporate BrdU (arrow) but not in AR-deleted prostate tumors (bottom), after administration of BrdU during later stages of regeneration. (**E**,**F**) Percentage of BrdU^{+} and BrdU^{-} cells among total YFP^{+} cells after injection of BrdU from days 1 through 4 (**E**) or days 11 through 14 (**F**) of regeneration. Error bars represent one standard deviation; the difference in **E** is not statistically significant (p=0.34, independent t-test), but is significant in **F** (p=0.027, independent t-test). This analysis excludes YFP^{+}AR^{+} cells that failed to undergo AR deletion in the experimental mice; full quantitation of all cell populations is provided in Figure 3 source data 1. (**G**) Schematic depiction of tissue recombination of lineage-marked CARNs with rat urogenital mesenchyme followed by renal grafting. (**H**) Analysis of grafts generated from lineage-marked CARNs (top) and AR-deleted CARNs (bottom); arrows in bottom panels indicate AR-expressing stromal cells surrounding the AR-negative prostate duct. Scale bars in **C**, **D,** and **H** correspond to 50 μm.

Figure 3 – source data. Quantitation of BrdU incorporation and renal grafting data.

Figure 4. Properties of cell lines established from CARNs and AR-deleted CARNs. (**A**) Morphology and marker expression of cell lines derived from single YFP^{+} cells from castrated and tamoxifen-treated control *Nkx3.1$^{CreERT2/+}$; R26R-YFP/+* mice and *Nkx3.1$^{CreERT2/+}$; Ar$^{flox/Y}$; R26R-YFP/+* mice. The APCA lines (top) and ADCA lines (bottom) show similar bright-field morphology, expression of YFP, Foxa1, and Ki67, as well as co-expression of CK8 and CK5,

but differ in expression of AR. (**B**) APCA and ADCA cell lines display similar cell growth at days 1, 2, 4, and 6 after plating in the absence or presence of DHT, as assessed by CellTiter-Glo assay. Results shown are from a single experiment with 5 technical replicates and are representative of 2 biological replicates after normalization with day 0 luminescent signal. (**C**) Colony formation by APCA and ADCA cell lines in the absence or presence of DHT. Results are from a single experiment with 3 technical replicates and are representative of 2 biological replicates. (**D**) Renal grafts generated from tissue recombinants of 100,000 APCA or ADCA cells with rat urogenital mesenchyme, and analyzed at 12 weeks. Bottom row shows APCA grafts treated with tamoxifen for 4 days at 7 weeks of growth to induce *Ar* deletion (bottom); arrows indicate cells that did not undergo *Ar* deletion after tamoxifen treatment. Scale bars in **A** and **D** correspond to 50 μm.

Figure 4 – figure supplement 1. Establishment of novel human prostate epithelial cell lines. (**A**) Flow-sorting strategy to eliminate $EpCAM^{-}E\text{-}cadherin^{-}$ cells from dissociated benign human prostate epithelial cells obtained from radical prostatectomies. (**B**) Bright-field images of a human prostate epithelial cell line at passage 3 and 6. (**C**) HPE cells broadly express AR and both luminal (CK8) and basal (CK5) markers, and have more limited expression of PSA and Ki67. Scale bars in **B** correspond to 100 μm, and in **C** to 50 μm.

Figure 4 – source data. Epithelial cell lines established from mouse and human prostate tissue.

Figure 5. Gene set enrichment analysis of the ADCA signature. (**A**) Selected biological pathways that are enriched in the ADCA versus APCA signature. (**B**) GSEA plot showing enrichment in the positive tail for a signature of AR-null mouse prostate epithelial cells. (**C**) Cross-species GSEA showing lack of enrichment with a signature based on isolated human prostate basal and luminal epithelial populations. (**D**-**F**) Cross-species GSEA comparing the

ADCA expression signature with three independent expression signatures based on tumor samples from human patients. NES: normalized enrichment score; *p*-value is calculated using 1000 gene permutations.

Figure 6. Deletion of AR alters the ability of CARNs to serve as a cell of origin for prostate cancer. (**A**) Prostate histology and marker expression in *Nkx3.1*$^{CreERT2/+}$*; Pten*$^{flox/flox}$*; R26R-YFP/+* (NP-CARN) and *Nkx3.1*$^{CreERT2/+}$*; Pten*$^{flox/flox}$*; Ar*$^{flox/Y}$*; R26R-YFP/+* (NPA-CARN) mice that have been castrated and tamoxifen-treated, followed by androgen-mediated regeneration for one month. Shown are representative images for hematoxylin-eosin staining (H&E) and immunofluorescence for YFP, AR, phospho-Akt (pAkt), E-cadherin (Ecad), Ki67, and cleaved caspase-3 (CC3). Arrows indicate occurrence of cell death (YFP/AR in NPA-CARN), proliferation (Ecad/Ki67), and apoptosis (Ecad/CC3). (**B**) Quantitation of Ki67$^+$ and CC3$^+$ positive cells in total Ecad$^+$ epithelial cells in NP-CARN and NPA-CARN prostates. Error bars represent one standard deviation; differences between groups are statistically significant as determined by independent t-test. (**C**) Prostate tumor histology and marker expression in *Nkx3.1*$^{CreERT2/+}$*; Pten*$^{flox/flox}$*; Kras*$^{LSL-G12D/+}$*; R26R-YFP/+* (NPK-CARN) and *Nkx3.1*$^{CreERT2/+}$*; Pten*$^{flox/flox}$*; Kras*$^{LSL-G12D/+}$*; Ar*$^{flox/Y}$*; R26R-YFP/+* (NPKA-CARN) mice that have been castrated and tamoxifen-treated, followed by androgen-mediated regeneration for one month. Arrows indicate cells undergoing proliferation (Ecad/Ki67) and apoptosis (Ecad/CC3). (**D**) Quantitation of Ki67$^+$ and CC3$^+$ positive cells in total Ecad$^+$ epithelial cells in NPK-CARN and NPKA-CARN prostates. Differences between groups are not statistically significant as determined by independent t-test (Ki67, p=0.724; CC3, p=0.507). (**E**) Focal neuroendocrine differentiation in NPKA-CARN tumors. Shown are H&E and immunohistochemical staining (IHC) of serial sections for Synaptophysin (Syn) and Aurora kinase A (Aurka), IHC for Foxa2 and Chromogranin A (ChrA), as well as immunofluorescence for YFP and Syn shown as an overlay and as individual channels; arrows indicate positive cells. (**F**) Quantitation of Syn$^+$ cells in total

epithelial cells in NPK-CARN and NPKA-CARN tumors. Scale bars for H&E and IHC in **A, C,** and **E** correspond to 100 μm, and in other panels to 50 μm.

Figure 6 – source data. Tumor phenotypes and marker quantitation.

Supplementary file 1. Primers and antibodies used in this study.

Figure 1

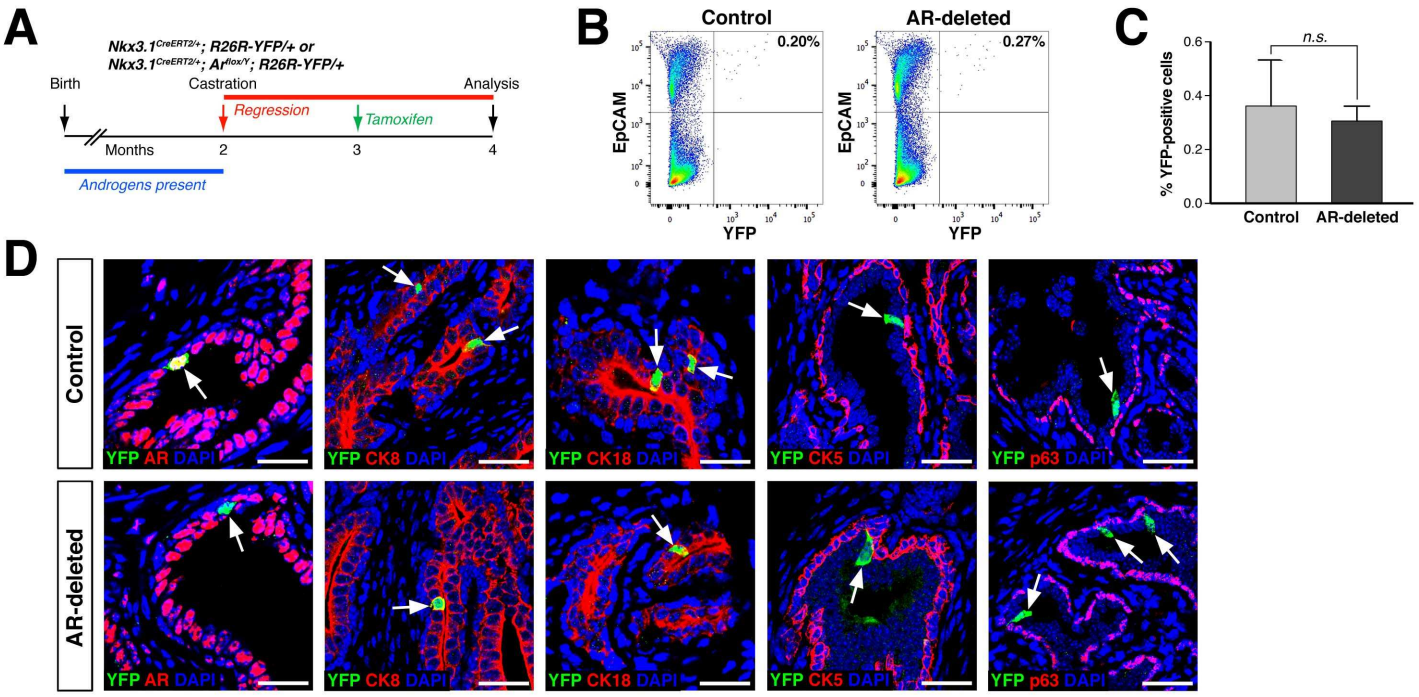
A
Nkx3.1CreERT2/+; R26R-YFP/+ or
Nkx3.1CreERT2/+; ARflox/Y; R26R-YFP/+
Birth
Castration
Analysis
Regression
Tamoxifen
Months
2
3
4
Androgens present
B
Control
AR-deleted
0.20%
0.27%
EpCAM
YFP
C
n.s.
% YFP-positive cells
0.6
0.4
0.2
0.0
Control
AR-deleted
D
Control
AR-deleted
YFP AR DAPI
YFP CK8 DAPI
YFP CK18 DAPI
YFP CK5 DAPI
YFP p63 DAPI

Figure 2

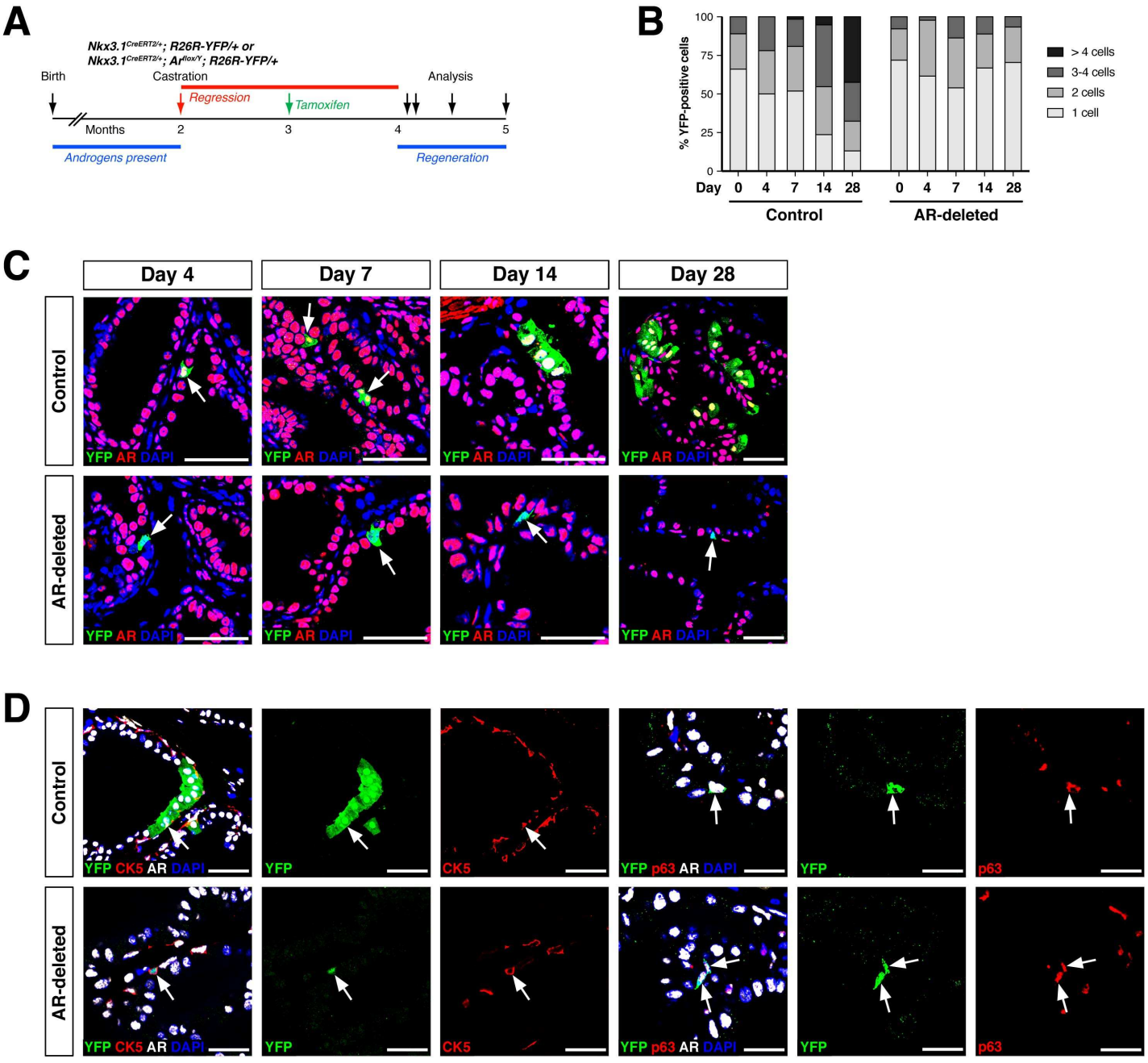
A
Nkx3.1CreERT2/+; R26R-YFP/+ or
Nkx3.1CreERT2/+; Arflox/Y; R26R-YFP/+
Birth
Castration
Analysis
Regression
Tamoxifen
Months
2
3
4
5
Androgens present
Regeneration
B
% YFP-positive cells
100
75
50
25
0
Day
0
4
7
14
28
Control
AR-deleted
> 4 cells
3-4 cells
2 cells
1 cell
C
Day 4
Day 7
Day 14
Day 28
Control
AR-deleted
YFP AR DAPI
D
Control
AR-deleted
YFP CK5 AR DAPI
YFP
CK5
YFP p63 AR DAPI
p63

Figure 3

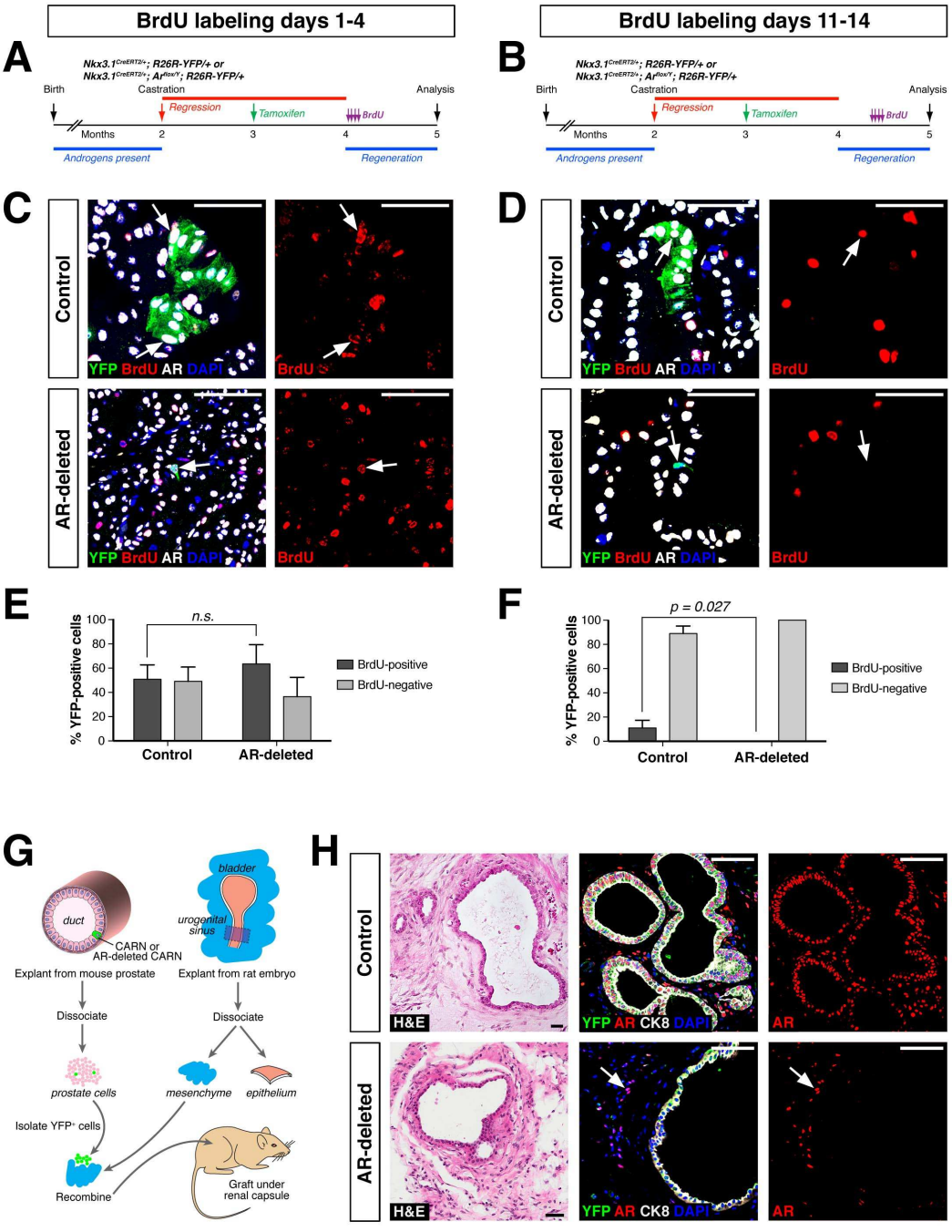
BrdU labeling days 1-4
BrdU labeling days 11-14
A
B
Nkx3.1CreERT2/+; R26R-YFP/+ or
Nkx3.1CreERT2/+; Arflox/Y; R26R-YFP/+
Birth
Castration
Analysis
Regression
Tamoxifen
BrdU
Months
2
3
4
5
Androgens present
Regeneration
C
D
Control
AR-deleted
YFP BrdU AR DAPI
BrdU
E
F
% YFP-positive cells
n.s.
p = 0.027
BrdU-positive
BrdU-negative
Control
AR-deleted
G
H
duct
CARN or
AR-deleted CARN
bladder
urogenital sinus
Explant from mouse prostate
Explant from rat embryo
Dissociate
prostate cells
mesenchyme
epithelium
Isolate YFP+ cells
Recombine
Graft under renal capsule
H&E
YFP AR CK8 DAPI
AR

Figure 4

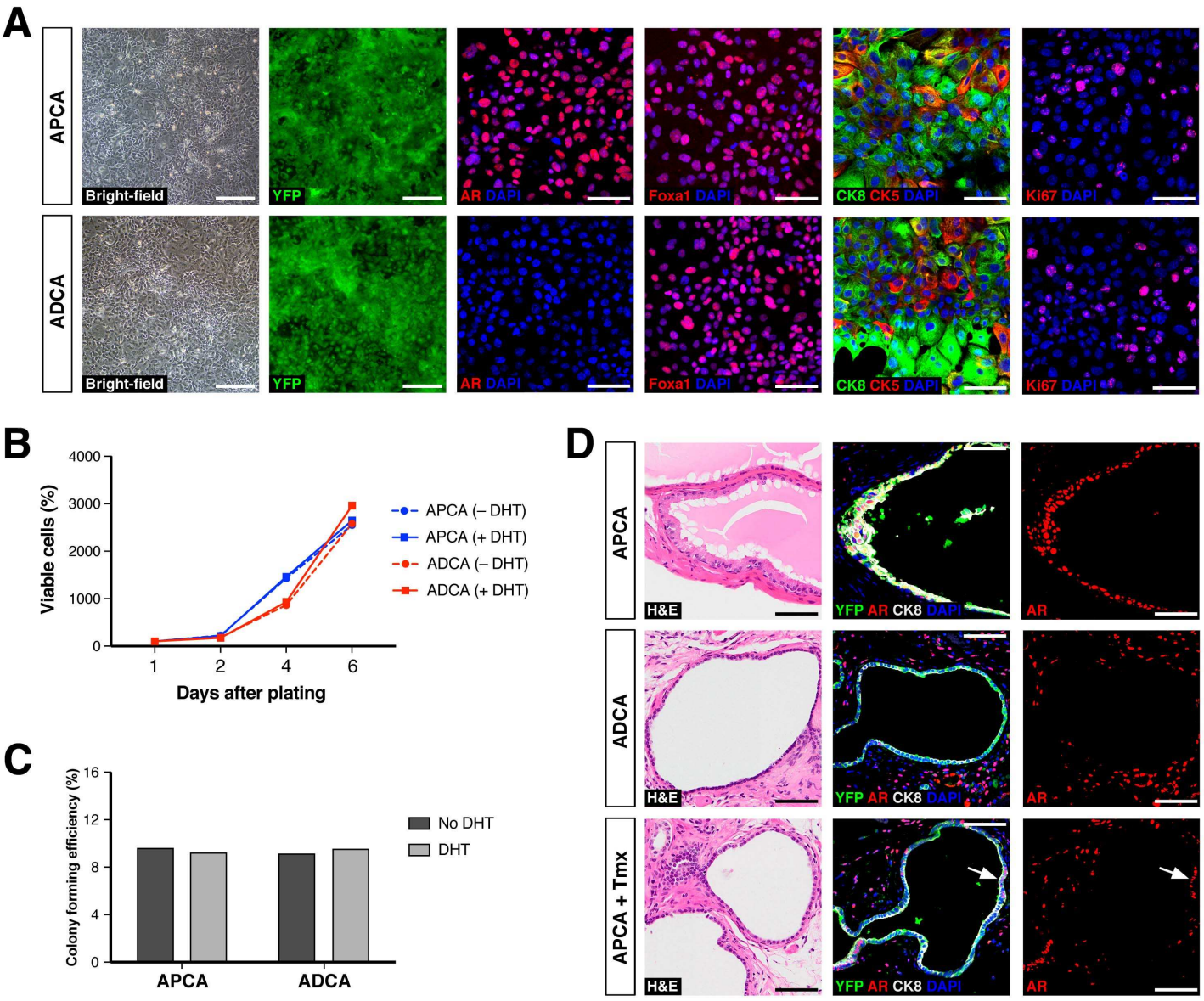
A
APCA
ADCA
Bright-field
YFP
AR DAPI
Foxa1 DAPI
CK8 CK5 DAPI
Ki67 DAPI
B
Viable cells (%)
4000
3000
2000
1000
0
1
2
4
6
Days after plating
APCA (– DHT)
APCA (+ DHT)
ADCA (– DHT)
ADCA (+ DHT)
C
Colony forming efficiency (%)
16
12
8
4
0
APCA
ADCA
No DHT
DHT
D
APCA
ADCA
APCA + Tmx
H&E
YFP AR CK8 DAPI
AR

Figure 4 – figure supplement 1

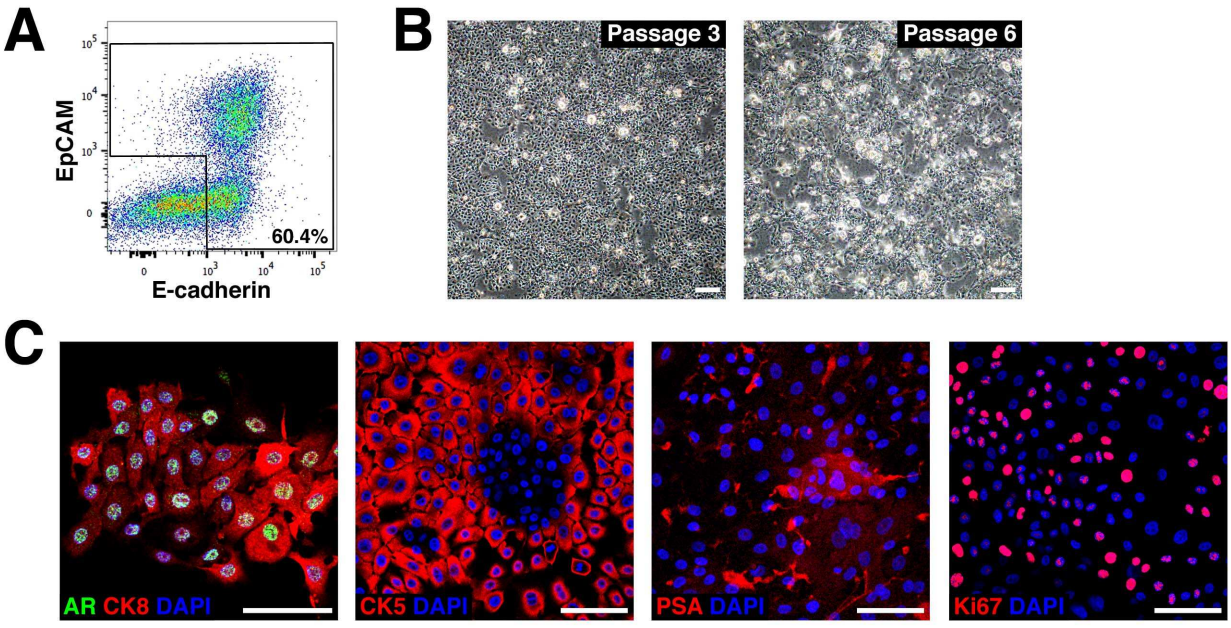

Figure 5

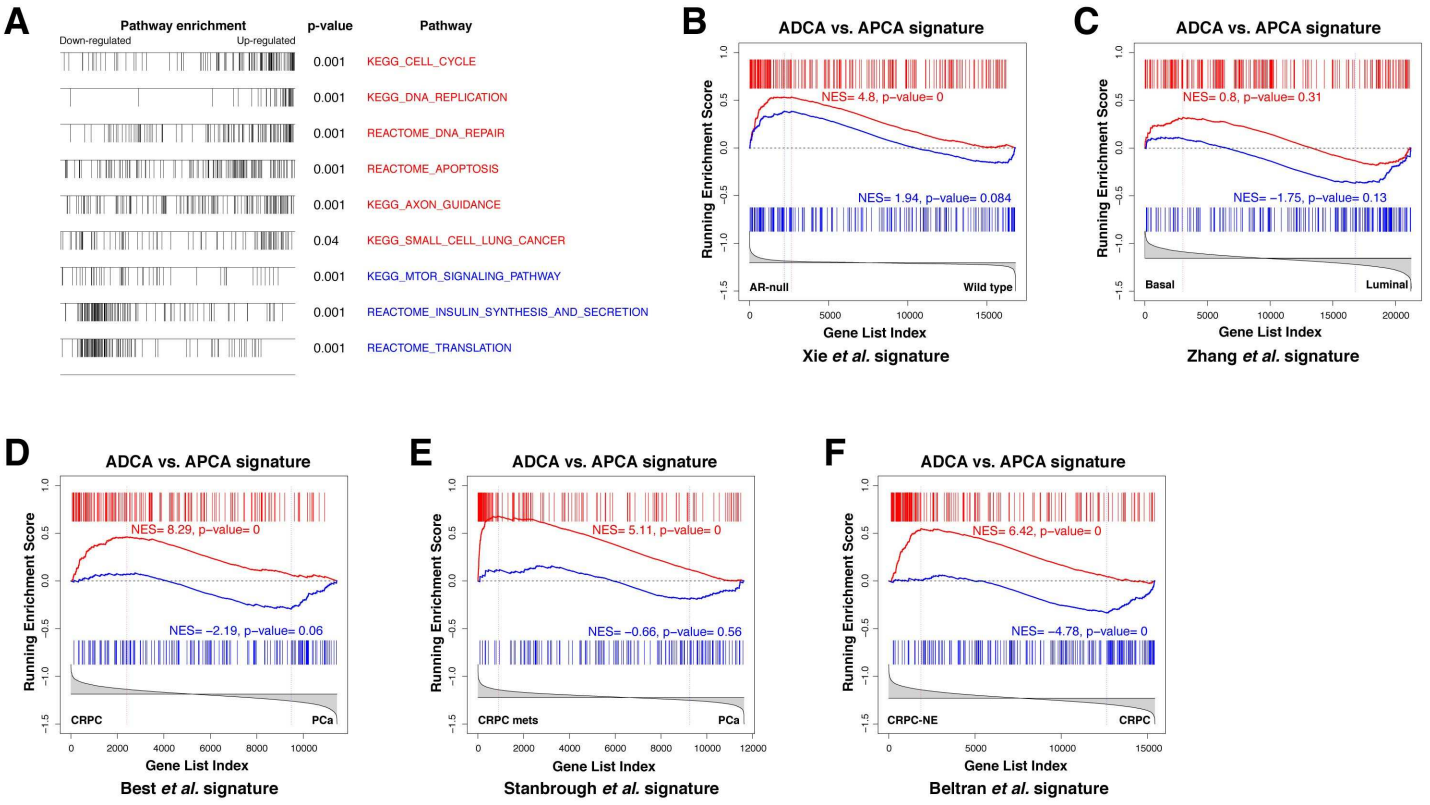
A
Pathway enrichment
Down-regulated
Up-regulated
p-value
Pathway
0.001 KEGG_CELL_CYCLE
0.001 KEGG_DNA_REPLICATION
0.001 REACTOME_DNA_REPAIR
0.001 REACTOME_APOPTOSIS
0.001 KEGG_AXON_GUIDANCE
0.04 KEGG_SMALL_CELL_LUNG_CANCER
0.001 KEGG_MTOR_SIGNALING_PATHWAY
0.001 REACTOME_INSULIN_SYNTHESIS_AND_SECRETION
0.001 REACTOME_TRANSLATION
B
ADCA vs. APCA signature
NES= 4.8, p−value= 0
NES= 1.94, p−value= 0.084
AR-null
Wild type
Running Enrichment Score
Gene List Index
Xie et al. signature
C
ADCA vs. APCA signature
NES= 0.8, p−value= 0.31
NES= −1.75, p−value= 0.13
Basal
Luminal
Running Enrichment Score
Gene List Index
Zhang et al. signature
D
ADCA vs. APCA signature
NES= 8.29, p−value= 0
NES= −2.19, p−value= 0.06
CRPC
PCa
Running Enrichment Score
Gene List Index
Best et al. signature
E
ADCA vs. APCA signature
NES= 5.11, p−value= 0
NES= −0.66, p−value= 0.56
CRPC mets
PCa
Running Enrichment Score
Gene List Index
Stanbrough et al. signature
F
ADCA vs. APCA signature
NES= 6.42, p−value= 0
NES= −4.78, p−value= 0
CRPC-NE
CRPC
Running Enrichment Score
Gene List Index
Beltran et al. signature

Figure 6

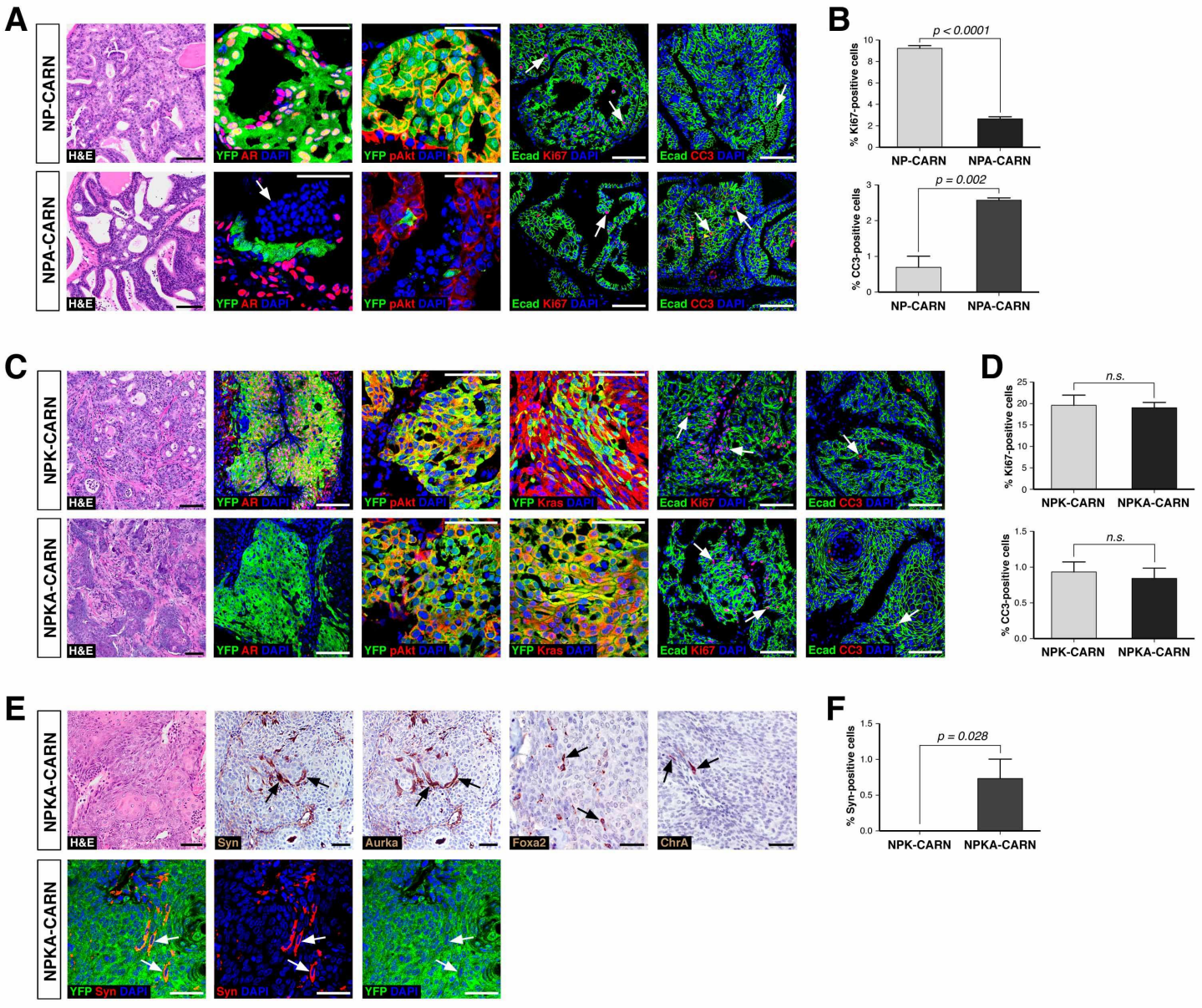
A
NP-CARN
NPA-CARN
H&E
YFP AR DAPI
YFP pAkt DAPI
Ecad Ki67 DAPI
Ecad CC3 DAPI
B
p < 0.0001
% Ki67-positive cells
NP-CARN
NPA-CARN
p = 0.002
% CC3-positive cells
C
NPK-CARN
NPKA-CARN
YFP Kras DAPI
D
n.s.
% Ki67-positive cells
% CC3-positive cells
E
Syn
Aurka
Foxa2
ChrA
YFP Syn DAPI
Syn DAPI
YFP DAPI
F
p = 0.028
% Syn-positive cells